https://doi.org/10.5194/egusphere-2026-2830
Preprint. Discussion started: 11 June 2026
© Author(s) 2026. CC BY 4.0 License.

Contrasting Detection and Attribution of Temperature and Precipitation Changes in the Western Mediterranean from CMIP6 DAMIP Experiments

Diego A. Campos[1,2], Matías E. Olmo[1], Pep Cos[1], Margarida Samsó[1],and Francisco J. Doblas-Reyes[1,3]

[1]Earth Sciences Department, Barcelona Supercomputing Center, Barcelona, Spain
[2]Facultat de Física, Universitat de Barcelona, Barcelona, Spain
[3]Catalan Institution for Research and Advances Studies, ICREA, Barcelona, Spain

Correspondence to: Diego A. Campos (diego.campos@bsc.es)

Abstract. The Western Mediterranean (WM) is a recognised climate change hotspot where regional temperature and precipitation trends reflect the interplay between anthropogenic forcing and strong internal variability. In this study, the detection and attribution of seasonal temperature and precipitation changes during 1951–2020 across climatically derived subregions of the WM is investigated using a multi-method framework and CMIP6 DAMIP single-forcing experiments. Prior to attribution, models were evaluated according to their ability to reproduce the observed spatial structure of regional trends, and a performance-based subset was selected for the analysis. Detection and attribution were assessed using complementary approaches, including the signal-to-noise ratio (SNR), the fraction of attributable risk (FAR), distribution-based comparisons, and an optimal fingerprinting additive decomposition framework. Results reveal a robust anthropogenic imprint on temperature trends across the WM. Forced temperature signals emerge clearly from internal variability in all subregions, with FAR values exceeding 0.95 in most cases. Greenhouse gas forcing is identified as the dominant driver of the observed warming, especially in summer, while anthropogenic aerosols exert a compensating cooling influence that partially offsets it. In contrast, precipitation trends remain largely within the bounds of internal variability. None of the detection approaches identifies a robust externally forced precipitation signal at the regional scale, and attribution results suggest that internal variability remains the primary driver of observed precipitation changes during the study period. These findings highlight the importance of subregional-scale attribution and model performance filtering in reducing uncertainties, providing a basis for future attribution studies in this highly vulnerable region.

1 Introduction

The Western Mediterranean (WM) is widely recognised as a climate change hotspot due to its accelerated warming signal and high socio-ecological vulnerability (Cos et al., 2022; Cramer et al., 2018; Tuel & Eltahir, 2020). Climate projections indicate regional warming rates exceeding the global average, together with a reduction in water availability, amplifying hydroclimatic stress in a region already characterised by hot, dry summers (Ali et al., 2022). In addition to rising

https://doi.org/10.5194/egusphere-2026-2830
Preprint. Discussion started: 11 June 2026
© Author(s) 2026. CC BY 4.0 License.

temperatures, projected changes in extremes, including more frequent heatwaves, rising sea levels and shifts in precipitation regimes, pose growing risks to ecosystems, water resources and key economic sectors across southern Europe and northern Africa (Cramer et al., 2018; Driouech et al., 2020).

Changes in regional temperature have been documented on decadal to multidecadal scales. Radiative forcing from anthropogenic greenhouse gases (GHG) is generally addressed as the main external factor of warming (Feng et al., 2022; Stott, 2003; Urdiales-Flores et al., 2023; Van Oldenborgh et al., 2009). Other processes may further modulate this warming signal. For instance, reductions in anthropogenic aerosol emissions since the late twentieth century have been associated with increased surface solar radiation ("brightening"), which may have contributed to accelerated warming in parts of the Mediterranean Basin since ~1980s (Nabat et al., 2014; Philipona et al., 2009; Schumacher et al., 2024). Land-atmosphere interactions, including soil moisture feedbacks during summer, may also amplify regional temperature changes and contribute to the spatial heterogeneity of warming across the region (Urdiales-Flores et al., 2023). Furthermore, analyses based on reanalysis data further indicate pronounced spatial and seasonal contrasts in the warming signal; for example, the strongest warming since the mid-twentieth century is found over the Iberian Peninsula and northern Africa during summer, where long-term trends account for more than 60% of the total temperature variance (Campos et al., 2025).

The WM region exhibits strong interannual to multidecadal precipitation variability. The sign and magnitude of precipitation trends vary depending on the period and season considered (Cherif et al., 2020; Mariotti et al., 2015). Despite this strong variability, a number of studies report evidence of a reduction in precipitation during the second half of the twentieth century. In particular, several analyses identify a decline in precipitation from the late 1950s onwards, most prominently during the cold season in the western part of the region (Campos et al., 2025; Hoerling et al., 2012; Seager et al., 2025; Xoplaki et al., 2004). However, the magnitude and spatial structure of this signal vary across datasets, and differences emerge depending on whether analyses rely on gridded datasets or atmospheric reanalysis products. Analyses of long observational records across the Mediterranean basin indicate that precipitation trends are highly dependent on the period analysed and show strong spatial heterogeneity (González-Hidalgo & Vicente-Serrano, 2025; Vicente-Serrano et al., 2025). While declines in winter precipitation are observed between roughly the 1950s and 2020s, several regions have experienced partial recovery or positive trends since the late twentieth century. Precipitation trends are often weak or statistically insignificant, suggesting that multi-decadal variability may dominate the observed hydroclimatic evolution of the WM (Lionello et al., 2012; Peña-Angulo et al., 2020; Vicente-Serrano et al., 2025).

The drivers of these hydroclimatic changes remain actively debated. Several studies emphasize the role of atmospheric circulation and internal variability (e.g., Campos et al., 2025; Mariotti et al., 2015; Olmo et al., 2024; Seager et al., 2025; Vicente-Serrano et al., 2025), while other studies argue that anthropogenic forcing may also play a role, consistent with climate model projections that indicate a robust decline in Mediterranean precipitation under continued radiative forcing

https://doi.org/10.5194/egusphere-2026-2830
Preprint. Discussion started: 11 June 2026
© Author(s) 2026. CC BY 4.0 License.

(Christidis & Stott, 2021, 2022; Hoerling et al., 2012; Mariotti et al., 2008; Olmo et al., 2025; Seager et al., 2014, 2024). Indeed, projections from successive generations of climate models consistently identify the Mediterranean basin as a climate change "hotspot", characterised by strong warming and a pronounced reduction in precipitation over the twenty-first century (Carvalho et al., 2022; Cos et al., 2022b; Giorgi & Lionello, 2008; Tarín-Carrasco et al., 2025). Reconciling these model projections with the complex and sometimes contradictory signals found in the historical record, therefore, remains an important challenge for understanding Mediterranean hydroclimate change.

Most attribution methods rely on climate model simulations (Allen & Stott, 2003; Hawkins & Sutton, 2012; Ribes et al., 2017; Ribes & Terray, 2013). According to the Sixth Assessment Report of the Intergovernmental Panel on Climate Change (AR6, IPCC), the model ensemble from the Coupled Model Intercomparison Project Phase 6 (CMIP6) reproduces the global temperature trends with biases small enough to support detection and attribution studies (IPCC, 2022). However, at a regional scale, models may exhibit errors in the spatial and temporal patterns of the response to external forcings, or in the representation of internal variability, which can result in a mismatch between observed and simulated climate responses (Ribes & Terray, 2013). This issue is particularly relevant for hydroclimatic variables such as precipitation, where CMIP models often struggle to reproduce the spatial patterns and magnitude of observed trends (Donat et al., 2023), partly due to the strong internal variability that characterises regional precipitation (Vicente-Serrano et al., 2022, 2025). As in other applications –such as statistical downscaling or formulating regional projections– filtering model ensembles based on specific performance criteria (e.g., realistic representation of climate variability or long-term trends) has proven useful for controlling spread (McSweeney et al., 2015; Merrifield et al., 2023; Olmo et al., 2025; Palmer et al., 2023). Applying similar filtering approaches in attribution studies may therefore help reduce the risk of misleading conclusions arising from model biases or unrealistic representations of regional variability.

This study aims to assess the detectability and attribution of recent hydroclimatic trends in the WM by analysing long-term seasonal trends in temperature and precipitation during the 1951-2020 period. This period is particularly relevant because it encompasses both the rapid increase in anthropogenic radiative forcing and the pronounced decadal variability documented in the WM hydroclimate (Mariotti et al., 2015). Given the strong spatial heterogeneity of observed climate trends across the Mediterranean basin, we focus on the analysis of sub-regional patterns within the WM (10°W–25°E, 33°–45°N), allowing the spatial structure of the observed changes to be examined in greater detail. This information is critical for interpreting recent hydroclimatic changes in the region and for assessing the robustness of projected future changes.

We apply multiple detection and attribution methodologies using simulations from the CMIP6, including the single-forcing experiments from the Detection and Attribution Model Intercomparison Project (DAMIP; Gillett et al., 2016), which have been relatively under-utilised in studies of Mediterranean hydroclimate. A consistent methodological framework is applied across variables, seasons, and sub-regions, enabling a direct comparison between temperature and precipitation responses.

https://doi.org/10.5194/egusphere-2026-2830
Preprint. Discussion started: 11 June 2026
© Author(s) 2026. CC BY 4.0 License.

The paper is organised as follows: Section 2 describes the data and methods used in the analysis; Sect. 3 presents the results of the different detection and attribution approaches; and Sect. 4 discusses the main findings in the context of previous literature.

2 Data and Methods

2.1 Data and model evaluation

For this study, monthly observational and simulated temperature and precipitation data have been used for the WM region (10°W-25°E; 33°-45°N; see Fig. 1i). For temperature, data were taken from the ECMWF Reanalysis version 5 (ERA5, Hersbach et al., 2020), Berkeley Earth (Rohde & Hausfather, 2020) and the Climate Research Unit version TS4.07 (CRU; Harris et al., 2020), while for precipitation, ERA5, CRU and the Global Precipitation Climatology Centre version 2022 (GPCC; Schneider et al., 2022) databases were used. Additionally, monthly temperature and precipitation data were derived from daily values for a set of ground stations obtained from the European Climate Assessment & Dataset (ECA&D) project (Klein Tank et al., 2002) and from the Daily Global Historical Climatology Network (GHCN-Daily) Version 3 (Menne et al., 2012) of NOAA-NCEI. A quality assessment was applied to the ground stations, retaining those with at least 70% of the years containing 70% of the daily records (Table S1 in the Supplement).

Monthly temperature and precipitation data were obtained from CMIP6 simulations. The Historical CMIP6 experiments span from 1850 to 2014 (Eyring et al., 2016); therefore, to complete the 1951-2020 period, the time series were extended using the SSP2-4.5 future scenario (Riahi et al., 2017). Additionally, a 500-year pre-industrial time series was obtained for each model from its piControl simulations. These simulations represent climate variability in the absence of external forcing and were used to estimate the magnitude of internal variability. Historical single-forced simulation data from the DAMIP experiments (Gillett et al., 2016) were used. The experiments considered in this study are the well-mixed greenhouse-gas-only (GHG-only), anthropogenic-aerosol-only (AAer-only), and natural-only (Nat-only) scenarios. For the AAer-only runs, BC, OC, SO2, SO4, NOx, NH3, CO, and NMVOC are considered. Similarly, for the Nat-only experiments, solar irradiance and stratospheric aerosols are included. For details, see Gillett et al. (2016). A total of 11 CMIP6 models providing the historical, DAMIP single-forcing experiments, and piControl simulations were selected for this study (Table 1). The number of simulations for each experiment and model is detailed in Table 1. All data from the models were regridded to a common 1° x 1° grid using linear interpolation with the Earth System Model Evaluation Tool (ESMValTool; Righi et al., 2020).

Table 1: CMIP6 models used in this study and the number of members.

Model	Native Resolution	Number of ensemble members				Reference
		Historical + SSP2-4.5	GHG-only	AAer-only	Nat-only	

https://doi.org/10.5194/egusphere-2026-2830
Preprint. Discussion started: 11 June 2026
© Author(s) 2026. CC BY 4.0 License.

ACCESS-CM2	1.25° x 1.875°	3	3	3	3	Ziehn et al. (2020)
ACCESS-ESM1-5	1.25° x 1.875°	3	3	3	3	Ziehn et al. (2020)
BCC-CSM2-MR	1.125° x 1.125°	3	3	3	3	Wu et al. (2021)
CNRM-CM6-1	1.406° x 1.406°	10	10	10	10	Voldoire et al., (2019)
CanESM5	2.812° x 2.812°	15	15	15	15	Swart et al. (2019)
FGOALS-g3	2.25° x 2.0°	3	3	3	3	Li et al. (2020)
HadGEM3-GC31-LL	1.25° x 1.875°	4	34	34	34	Andrews et al. (2020)
IPSL-CM6A-LR	1.25° x 2.5°	6	10	10	10	Boucher et al. (2020)
MIROC6	1.406° x 1.406°	10	10	10	10	Tatebe et al. (2019)
MRI-ESM2-0	1.125° x 1.125°	5	5	5	5	Yukimoto et al. (2019)
NorESM2-LM	1.25° x 3.75°	3	3	3	3	Bentsen et al. (2013)

To account for the heterogeneity in temperature and precipitation trends in the WM, the region was divided into nine sub-regions following Campos et al. (2025) (Fig. 1i). This clustering was derived from monthly temperature and precipitation data that were first reduced via empirical orthogonal functions (EOFs). EOFs retaining 90% of the total temporal variance were selected and used as input for a k-means clustering procedure. Monthly time series for each cluster were calculated using the median of all grid cells within the cluster. To evaluate whether both models and observational datasets can distinguish these sub-regions, the rank-sum test (Mann & Whitney, 1947) was applied to the monthly temperature and precipitation distributions with a 5% significance level. This analysis was complemented by a comparison of sub-regional means and variances to further characterise the differences among clusters.

Sub-regional trends, which summarise the spatial patterns of temperature and precipitation across the WM, provide a basis for assessing models' ability to reproduce these patterns. Taylor diagrams were drawn to quantify the statistical similarity between the ERA5-based reference pattern and the different models, reporting Pearson correlation, normalised standard deviation, and root-mean-square error (Taylor, 2001), allowing the selection of models that better reproduce the observed spatial variability before performing attribution analyses. The analysis included n = 36 data points (nine regions × four seasons), with ERA5 serving as the observational reference and the ensemble mean of each model as the input (Fig. S1 in the Supplement). ERA5 was used in this step because the regionalisation framework of Campos et al. (2025) was originally derived from this dataset. The subsequent detection and attribution analyses do not rely exclusively on ERA5 and instead consider multiple observational products. Although ERA5 does not directly assimilate precipitation observations, previous studies have shown that it reproduces the interannual variability and long-term trends of Mediterranean precipitation reasonably well when compared with observation-based datasets (Campos et al., 2025; Seager et al., 2025), despite spatial discrepancies.

Based on the results of the Taylor diagrams, a subset of models was selected for temperature and precipitation for subsequent detection and attribution analyses.

https://doi.org/10.5194/egusphere-2026-2830
Preprint. Discussion started: 11 June 2026
© Author(s) 2026. CC BY 4.0 License.

2.2 Detection and attribution methods

To assess whether signals of temperature and precipitation change have emerged from climate models' internal variability in recent decades, a signal-to-noise ratio (SNR) framework was applied (e.g., Chemke & Coumou, 2024). The signal was defined as the ensemble-mean simulated trend in temperature and precipitation from 1951 to each year over the 1951–2020 period. Trends were estimated using Sen's slope derived from the Mann-Kendall test (Wilks, 2019). The noise was estimated from pre-industrial control simulations as the standard deviation of trends of the same length as the signal, thereby accounting for the dependence of internal variability of the trend for a specific time series length. These trends were computed using all possible overlapping segments within each control simulation. The SNR was calculated as the ratio of the slope of the ensemble-mean forced trend to the standard deviation of slopes from all overlapping segments of the same length in the control simulations. Additionally, a time of emergence (ToE) approach (Hawkins & Sutton, 2012) was used to determine when the simulated trends emerge from internal variability. The ToE was defined as the first year in which the magnitude of the signal consistently exceeded twice the standard deviation of internal variability ($|SNR| > 2$).

To assess whether climate models reproduce the magnitude and sign of observed sub-regional trends, a classification framework based on Knutson & Zeng (2018) was applied. For each region, season, and trend length, observed trends were compared with the distributions of trends simulated under natural-only (Nat-only) and all-forcing (Historical) experiments. Detection was defined following Knutson & Zeng (2018) as the combination of statistical distinguishability from natural variability and consistency in sign with the simulated forced response. In this framework, the observed trend is evaluated against distributions of model-simulated trends: Nat-only simulations are used to estimate the range of trends arising from internal variability, while the multi-model ensemble mean of the Historical simulations represents the expected forced response. Specifically, an observed trend was considered detectable if it lies outside the 5th–95th percentile range of the Nat-only distribution and has the same sign as the multi-model ensemble mean of the all-forcing simulations. Trends that do not meet these criteria were classified either as not detectable (category 0) or as sign-inconsistent cases (categories ±4). The sign of each category (+ or –) indicates the direction of the observed trend (positive or negative). To assess detectable trends, consistency with model-simulated forced responses was further evaluated by comparing them with the all-forcing distribution and the ensemble-mean response. Categories ±2 correspond to detectable trends that are consistent with the range of simulated all-forcing responses. Categories ±1 correspond to detectable trends that are weaker than the ensemble-mean forced response but remain distinguishable from natural variability. Categories ±3 identify detectable trends that are inconsistent with the all-forcing distribution, indicating discrepancies in magnitude. Categories ±4 correspond to cases where the observed trend has the opposite sign to the simulated forced response, representing a fundamental model–observation inconsistency. See Supplementary Figure 1 for a diagram illustrating these criteria.

https://doi.org/10.5194/egusphere-2026-2830
Preprint. Discussion started: 11 June 2026
© Author(s) 2026. CC BY 4.0 License.

To attribute observed trends in the WM to anthropogenic emissions, the fraction of attributable risk (FAR) framework (Stott et al., 2016) was applied to the sub-regional trends. Trends over the 1951-2020 period were computed for all ensemble members from the selected model subsets, using both the Historical and Nat-only experiments. For each experiment, Gaussian distributions were fitted to the ensemble of simulated trends. These distributions were used to estimate the probability of exceedance of the observed trends (from ERA5, CRU and Berkeley Earth for temperature, and ERA5, CRU and GPCC for precipitation), accounting for the sign of the trend (i.e., upper-tail probabilities for positive trends and lower-tail probabilities for negative trends). The probability under all forcings is denoted PALL, and under Natl-only forcing, PNAT. The FAR was then computed as FAR = 1 - PNAT / PALL, representing the fraction of the probability of occurrence attributable to anthropogenic forcing. A FAR greater than 0.5 indicates that simulations including anthropogenic forcing produce trends of this magnitude at least twice as frequently as simulations with natural forcing only. To account for sampling uncertainty, a bootstrap resampling procedure was applied to the model ensembles, and FAR estimates are reported as the median and associated percentile ranges across bootstrap realisations. To further assess the robustness of the FAR estimates, a Kolmogorov-Smirnov (KS) test was applied to the distributions of trends from the Historical and Nat-only simulations. The null hypothesis is that the two samples are drawn from the same underlying distribution (Wilks, 2019).

The classification framework provides a qualitative assessment of detectability and model consistency, while the FAR analysis offers a complementary probabilistic quantification of anthropogenic influence on the observed trends.

2.3 Contributions by external forcings

To investigate the contributions of individual external forcings on recent trends over the WM (in this case, greenhouse gases, anthropogenic aerosols, and natural forcings), a statistical detection and attribution framework based on additive decomposition and maximum likelihood estimation was used. This approach was proposed by Ribes et al. (2017) as an alternative to the optimal fingerprints based on linear regression (e.g., Allen & Stott, 2003; Hegerl et al., 2011; Ribes et al., 2013) and has been applied in studies at the sub-regional scale (De Abreu et al., 2019).

The method is based on the additivity assumption, in which Y^* represents the true observed climate response of the climate system to a number (nf) of true individual external forcings (Xi^*) taken together as:

$$Y^* = \sum_{i=1}^{nj} Xi^* \quad (1)$$

$$Y = Y^* + \varepsilon y, \qquad \varepsilon y \sim N(0, \Sigma y) \quad (2)$$

$$Xi = Xi^* + \varepsilon x, \qquad \varepsilon x \sim N(0, \Sigma x_i) \qquad i = 1, \ldots, nf \quad (3)$$

https://doi.org/10.5194/egusphere-2026-2830
Preprint. Discussion started: 11 June 2026
© Author(s) 2026. CC BY 4.0 License.

where Y is the observation vector with y observational uncertainty, and Xi is the simulated individual forcing vector with x model uncertainty, with their respective covariance matrices y and x_i. It is assumed that observational uncertainty arises from internal variability, while model uncertainty includes both internal variability and structural model uncertainty. Both uncertainty distributions are assumed Gaussian, so Xi^* and Y^* can be estimated using maximum likelihood estimators (MLE, $\hat{Y}^*$ and $\widehat{Xi}^*$) as described in Ribes et al. (2017). As in De Abreu et al. (2019), the consistency with internal variability, as well as with different sets of external forcings, is assessed using a χ^2 test (Wilks, 2006).

Trends are estimated from the best estimates $\hat{Y}^*$ and $\widehat{Xi}^*$. Confidence intervals are then constructed by computing trends from 4000 realisations drawn from multivariate normal distributions, using the mean and covariance matrices of $\hat{Y}^*$ and $\widehat{Xi}^*$, respectively.

In this study, the observation vector Y was constructed from observational datasets by averaging across them to reduce dataset-specific uncertainties and enhance the robustness of the estimated signal. The simulated individual forcing vectors Xi were obtained from the DAMIP experiments, using the model subset. The number of ensemble members per model is provided in Table 1. Similarly, the internal variability matrix (Z) was obtained from the pre-industrial control runs and is used to obtain the covariance matrices of internal variability. The vectors Y, Xi, Z were then obtained using the decadal averages for each season and sub-region in the WM region.

The analysis was performed using the Python package described in De Abreu et al. (2019), which is publicly available on GitHub (https://github.com/rafaelcabreu/attribution/).

3 Results

Observed and simulated temperature and precipitation trends over the Western Mediterranean (WM) for 1951-2020 are shown in Fig. 1. For temperature (Fig. 1a-d), both reanalysis (ERA5) and station data consistently indicate widespread warming across the domain, with stronger trends in summer (JJA) than in winter (DJF). The spatial pattern is not fully homogeneous; the most pronounced warming is found over the Iberian Peninsula and North Africa, although some differences in magnitude between ERA5 and station observations in some regions are observed. Despite these differences, the overall agreement in the sign of the trends is robust across observational datasets. In contrast, the multi-model ensemble mean exhibits a spatially smoother warming pattern, with positive trends across the entire WM in both seasons and an amplified summer signal. This homogenization is consistent with the averaging across models, which tends to damp regional contrasts. Model agreement for temperature is high across most of the domain, with the ensemble-mean signal generally exceeding the inter-model spread, indicating a robust and spatially coherent warming response (Fig. 1b,d).

https://doi.org/10.5194/egusphere-2026-2830
Preprint. Discussion started: 11 June 2026
© Author(s) 2026. CC BY 4.0 License.

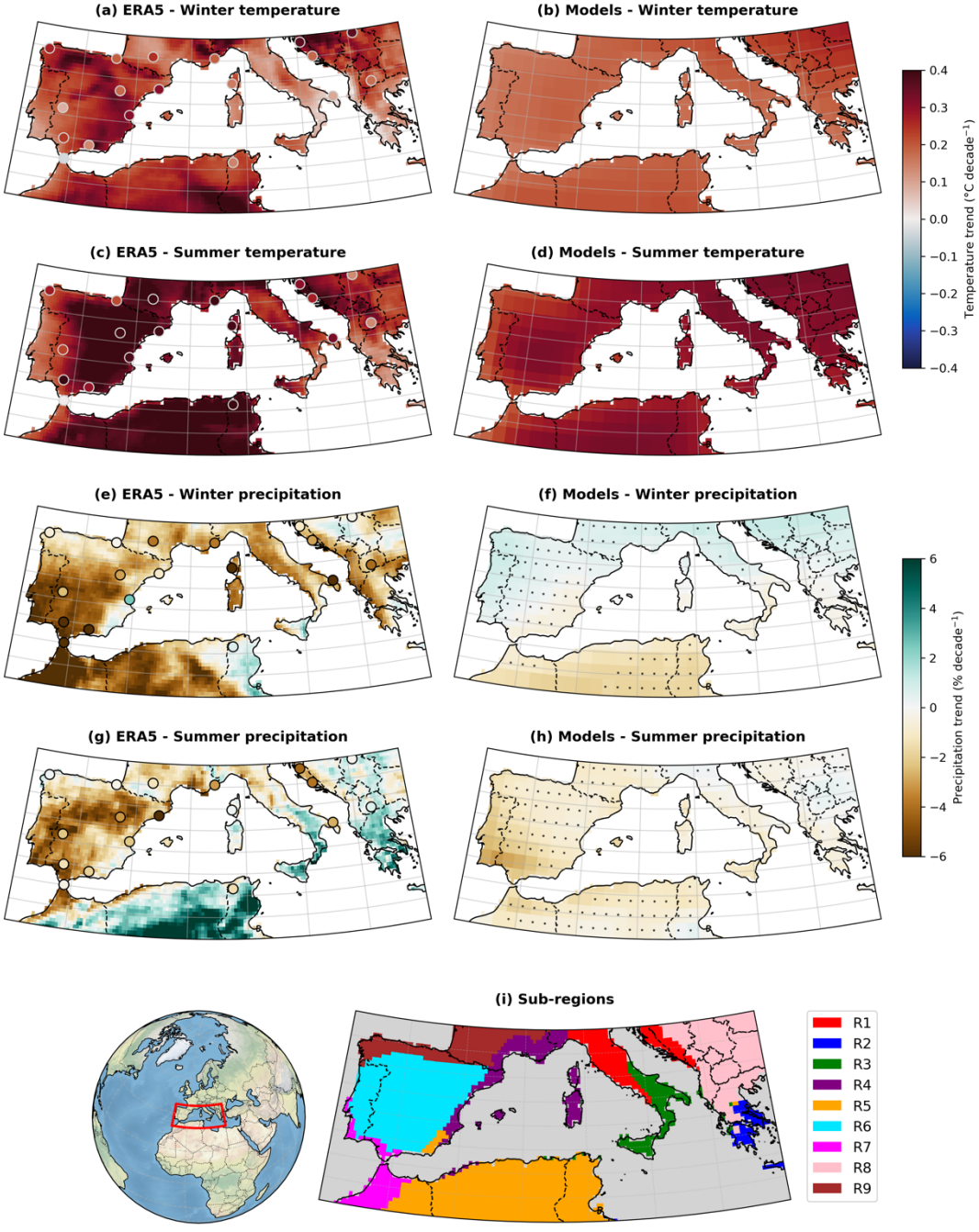

Figure 1: Observed and simulated trends of temperature and precipitation over the Western Mediterranean (WM) for the 1951–2020 period. Panels (a–d) show temperature trends and panels (e–h) precipitation trends. Observations are shown in the left column ((a), (c), (e), (g)), with ERA5 represented by shading and ground-based station data by coloured circles. Simulated trends are shown in the right column ((b), (d), (f), (h)) as the multi-model ensemble mean. In the model panels, regions where the ensemble-mean trend does not exceed the inter-model spread are masked, indicating low agreement among models and reduced

https://doi.org/10.5194/egusphere-2026-2830
Preprint. Discussion started: 11 June 2026
© Author(s) 2026. CC BY 4.0 License.

robustness of the simulated signal. Panels (a–b) and (e–f) correspond to winter (DJF), while panels (c–d) and (g–h) correspond to summer (JJA). Panel (i) shows the sub-regional clustering of the WMed used in this study, following Campos et al. (2025).

For precipitation (Fig.1e-h), the trends exhibit a more heterogeneous spatial pattern than those for temperature. In winter, both ERA5 and station data indicate a predominance of drying signals, especially over the western WM, including the Iberian Peninsula and North Africa, where agreement between datasets is the highest. In summer, however, precipitation trends are more spatially variable, with alternating regions of drying and wetting and reduced consistency between ERA5 and station data, highlighting the strong regional variability of precipitation in the WM. The simulated precipitation response differs more markedly from observations than for temperature. In winter, the ensemble mean shows a dipole-like structure, with wetting trends in the northern WM and drying in the south, in contrast to the more uniformly negative observed tendencies (Fig. 1f,h). Moreover, large areas are masked due to low model agreement, indicating substantial inter-model spread. In summer, models simulate a more spatially coherent drying signal, particularly over the Iberian Peninsula; however, this contrasts with the patchier and regionally heterogeneous patterns seen in observations.

To further characterise these differences at the regional scale, the WM domain is partitioned into sub-regions (Fig. 1i), which are analysed in detail in Fig. 2.

Temperature trends are consistently positive across nearly all regions and datasets (ERA5, CRU, Berkeley Earth), with stronger warming in summer than in winter (Fig. 2a-b). In winter, however, some regional differences emerge. In particular, region R2 does not exhibit significant trends in any observational dataset, and even shows weak negative (non-significant) trends in CRU data (Fig. 2a). In summer, the magnitude and spatial distribution of warming vary across observational products. ERA5 shows the strongest warming over R5 and R6, whereas CRU and Berkeley Earth do not consistently reproduce this sub-regional amplification (Fig. 2b). Overall, the observational datasets display substantial spatial variability in the magnitude of warming across the WM sub-regions, highlighting the observational uncertainty within the WM. In contrast, models simulate a more spatially homogeneous warming signal, with significant positive trends dominating across most regions in both seasons. While models broadly capture the widespread nature of warming, they show limited agreement on the relative magnitude of trends between sub-regions, failing to consistently reproduce the spatial contrasts seen in observations (Fig. 2a-b). This may partly reflect the relatively coarse spatial resolution of global climate models (Table 1), which limits their ability to resolve fine-scale regional processes influencing sub-regional warming patterns.

Precipitation trends exhibit substantially greater spatial variability and lower consistency across datasets (Fig. 2c-d). In winter, all observational datasets (ERA5, CRU, and GPCC) indicate predominantly negative trends across the WM. At the scale of the full domain (WM), ERA5 and CRU show significant negative trends, while CRU additionally indicates significant trends in R5. Notably, all three datasets agree on significant drying in region R7 (southwestern Iberian Peninsula

https://doi.org/10.5194/egusphere-2026-2830
Preprint. Discussion started: 11 June 2026
© Author(s) 2026. CC BY 4.0 License.

290 and northern Africa), making it one of the most robust subregional signals (Fig. 2c). In summer, precipitation trends are more heterogeneous. ERA5 does not show significant trends in any subregion, whereas CRU indicates significant drying in R4, R6, and R7. GPCC also shows significant negative trends in R6 and R7. In contrast, regions R2 and R3 display weak positive (non-significant) tendencies across datasets (Fig. 2d). Model results for precipitation are highly variable in both seasons, with no consistent tendency towards either drying or wetting across regions. This lack of agreement persists even in
295 regions where observational datasets show coherent signals, such as winter drying in R7. The large inter-model spread and inconsistency in the sign and significance of trends highlight substantial uncertainty in the simulated precipitation response, with potential implications for the robustness of subsequent attribution analyses (Fig. 2c-d).

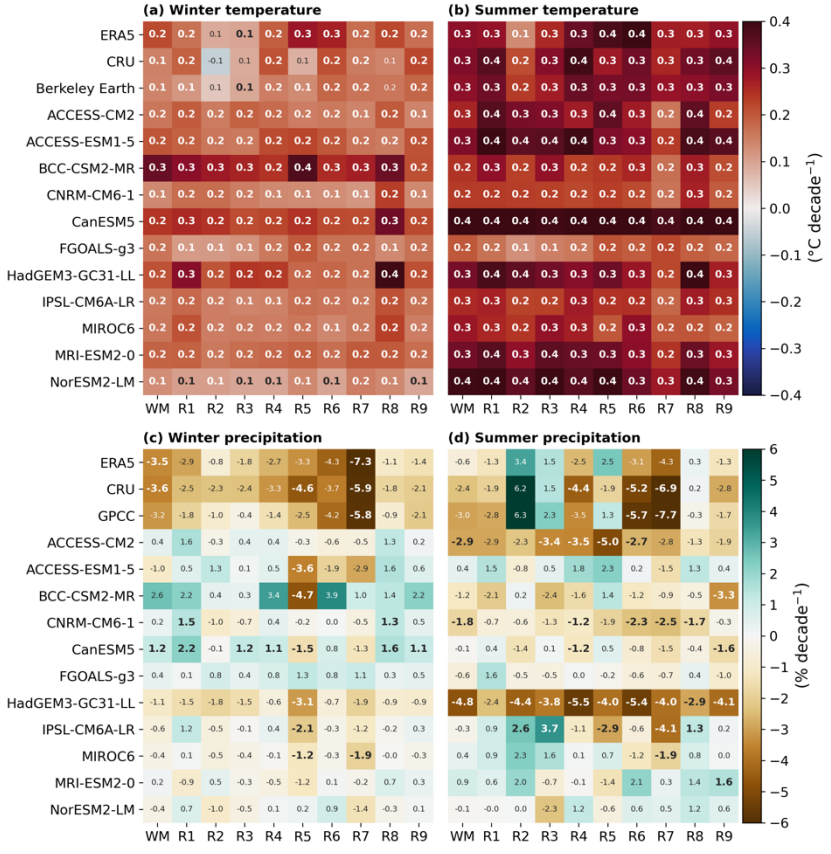

300 **Figure 2: Sub-regional trends in temperature and precipitation across the Western Mediterranean (WM). Columns represent the WM sub-regions defined in Figure 1i, while rows correspond to observational datasets (ERA5, CRU, Berkeley Earth for temperature; ERA5, CRU, GPCC for precipitation) and individual CMIP6 models. Values indicate linear trends over the 1951–2020 period for (a) winter temperature, (b) summer temperature, (c) winter precipitation, and (d) summer precipitation. Statistically significant trends are highlighted in bold.**

305

https://doi.org/10.5194/egusphere-2026-2830
Preprint. Discussion started: 11 June 2026
© Author(s) 2026. CC BY 4.0 License.

Building on the regional discrepancies identified above, in the next section, models are evaluated according to their ability to reproduce the observed spatial patterns of temperature and precipitation trends. This assessment is used to define a subset of models for the subsequent detection and attribution analysis.

3.1 Model selection

To ensure a consistent basis for the detection and attribution analysis, models were first evaluated according to their ability to reproduce the observed spatial patterns of sub-regional trends (Fig. 2). ERA5 was used as the reference dataset, as the regionalisation framework applied in this study was originally derived from this dataset (see Sect. 2.1). The ensemble mean of each model was considered (see Sect. 2.1). All seasons were considered in the analysis (Fig. S2 in the Supplement).

The evaluation for temperature trends is summarised in Fig. 3. Despite the overall agreement in the sign of warming across the WM, models show limited skill in reproducing the spatial distribution of sub-regional trends. Correlations between observed and simulated seasonal trends remain below 0.6 for all models (Fig. 3a), indicating substantial discrepancies in the representation of regional contrasts. In addition, most models exhibit a normalised standard deviation below one, reflecting an underestimation of the spatial variability of temperature trends. These deficiencies are consistent with the homogenised warming patterns identified in Figure 1 and the reduced spatial contrasts seen in Fig. 2. However, it is worth noting that the use of the ensemble means rather than individual ensemble members reduces internal variability and may smooth the magnitude of simulated trends, which could partly contribute to the differences with the reference dataset.

For precipitation, model performance is further degraded. Correlations do not exceed 0.5 for any model, and the spread in simulated trends is large across regions and seasons (Fig. 4a). This confirms the strong inter-model variability and the limited ability of models to reproduce the observed spatial structure of precipitation trends highlighted in Fig. 2. As for temperature, these discrepancies do not arise from an inability to represent the mean climate or the distinction between sub-regions (Fig. S3 and S4 in the Supplement), but rather from limitations in simulating long-term trend patterns.

Given the generally low skill across models –particularly for precipitation– a pragmatic selection criterion based on the sign of the spatial correlation ($r > 0$) was adopted. This ensures that only models capturing, at a minimum, the regional-scale spatial structure of observed trends are retained for attribution. Based on this criterion, 9 out of 11 models are selected for temperature, excluding BCC-CSM2-MR and HadGEM3-GC31-LL. For precipitation, 7 models satisfy this condition: ACCESS-ESM1-5, CanESM5, FGOALS-g3, HadGEM3-GC31-LL, IPSL-CM6A-LR, MIROC6, and MRI-ESM2-0 (Fig. 3a and 4a).

https://doi.org/10.5194/egusphere-2026-2830
Preprint. Discussion started: 11 June 2026
© Author(s) 2026. CC BY 4.0 License.

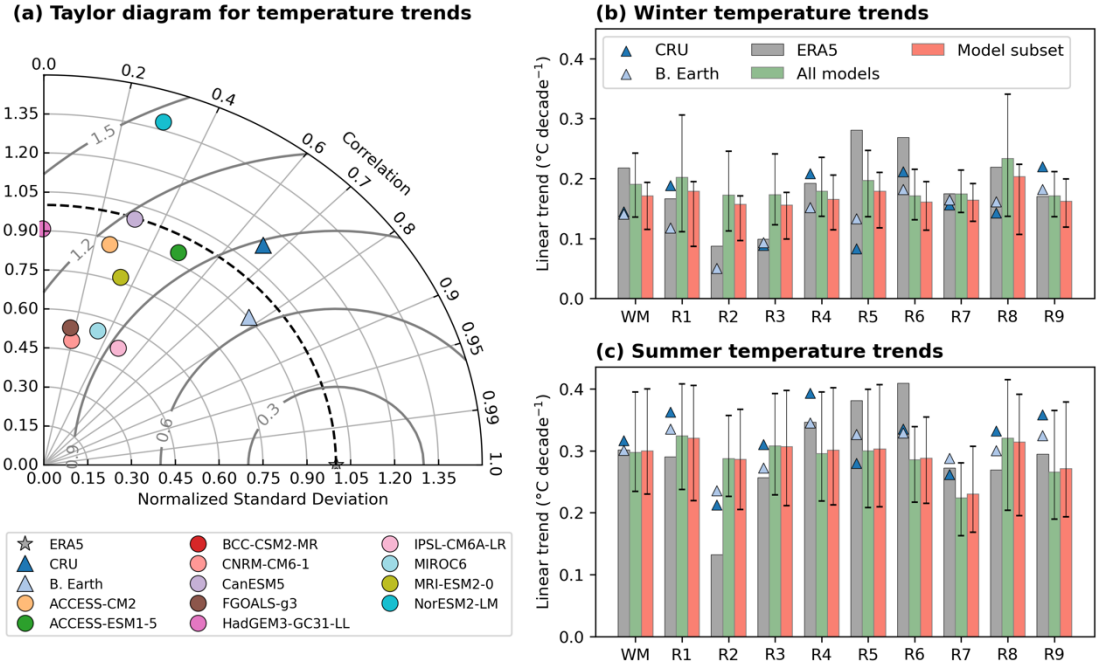

Figure 3: Model evaluation for temperature trends over the Western Mediterranean. (a) Taylor diagram based on seasonal sub-regional trends. The grey star denotes ERA5 as the reference dataset, triangles represent other observational datasets, and circles represent individual models. (b) Sub-regional winter temperature trends from ERA5 (grey), all models (green), and the selected model subset (orange). Triangles indicate trends from additional observational datasets. Coloured bars show the mean trend for each group, and vertical lines indicate the 10th–90th percentile range. (c) Same as (b), but for summer.

The use of the model subset leads to clearer modifications in the representation of precipitation trends than from temperatures. In winter, the subset better captures the observed drying signal in key regions such as R5 and R7, reducing inter-model spread and correcting the sign of the ensemble-mean trend (Fig. 4b). Similar modifications are found in summer, particularly in R7, where the subset more consistently reproduces negative trends (Fig. 4c). In other regions, more moderate gains are observed, including a better representation of trend magnitude and reduced dispersion across models, generally bringing the simulated trends closer to the observational estimates. For temperature, the impact of the model selection is more limited, with only marginal differences relative to the full ensemble in both seasons (Fig. 3b-c), reflecting the already coherent warming signal across models.

However, some discrepancies persist in specific regions and seasons. In particular, models still struggle to reproduce observed trends in regions such as R2 for winter temperature and in parts of the domain for precipitation. It should be noted, however, that observational datasets themselves exhibit non-negligible differences in the magnitude and spatial distribution of regional trends (Fig. 4). These remaining limitations highlight the uncertainty associated with regional-scale trends and

https://doi.org/10.5194/egusphere-2026-2830
Preprint. Discussion started: 11 June 2026
© Author(s) 2026. CC BY 4.0 License.

are accounted for in the interpretation of the subsequent detection and attribution results, with low-confidence regions masked where appropriate.

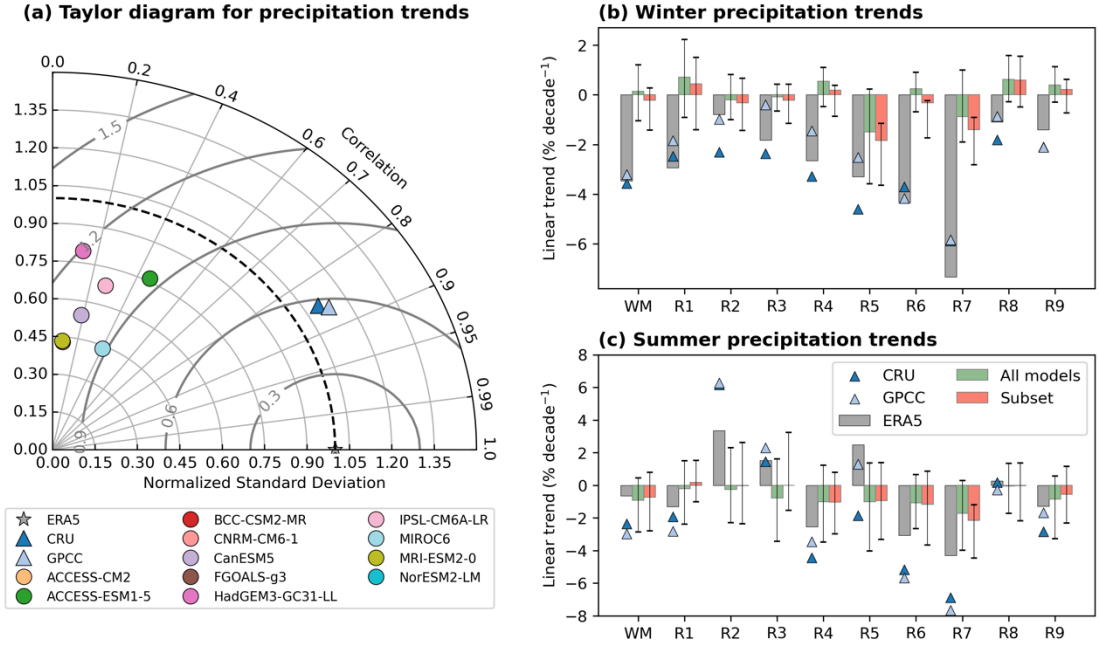

Figure 4: As in Figure 3, but for precipitation trends.

3.2 Detection and attribution of temperature trends

Based on the SNR and ToE approaches, the emergence of forced temperature trends from internal variability was assessed across the WM sub-regions. The emergence of temperature trends from internal variability is robust across all regions of the WM (Fig. 5a-b). The SNR exceeds the emergence threshold (|SNR| > 2) in all regions and for both seasons, indicating that the simulated forced signal is clearly distinguishable from internal variability. Emergence generally occurs earlier in summer, around the early 2000s (50-year-long trends), whereas in winter it is slightly delayed. It should be noted that this framework, on its own, assesses the detectability of the forced signal within the model ensemble, rather than providing direct attribution of observed trends.

The categorical classification framework places the observed trends in the context of the model-simulated distributions (Fig. 5c–d). Most regions are classified as Category +2, indicating detectable observed trends that are consistent with the range of model responses under all forcings. Exceptions are limited and largely confined to winter. In R2, observed trends are classified as non-detectable (Category 0) for ERA5 and Berkeley Earth, and as sign-inconsistent (Category -4) for CRU,

https://doi.org/10.5194/egusphere-2026-2830
Preprint. Discussion started: 11 June 2026
© Author(s) 2026. CC BY 4.0 License.

reflecting the weak or negative observed trends in this region. Additional non-detectable cases (Category 0) occur in R3 (CRU and Berkeley Earth) and R5 (CRU). Additionally, R6 in ERA5 is classified as Category +3, indicating a detectable trend that lies outside the model-simulated range and suggesting a potential underestimation of warming magnitude by models (Fig. 5c). In summer, classifications are almost exclusively Category +2, with the only exception being R2 in ERA5, which falls into Category +1, indicating a detectable but weaker-than-simulated response (Fig. 5d). This framework provides a useful way to interpret the detectability and consistency of observed trends relative to the range of model-simulated responses.

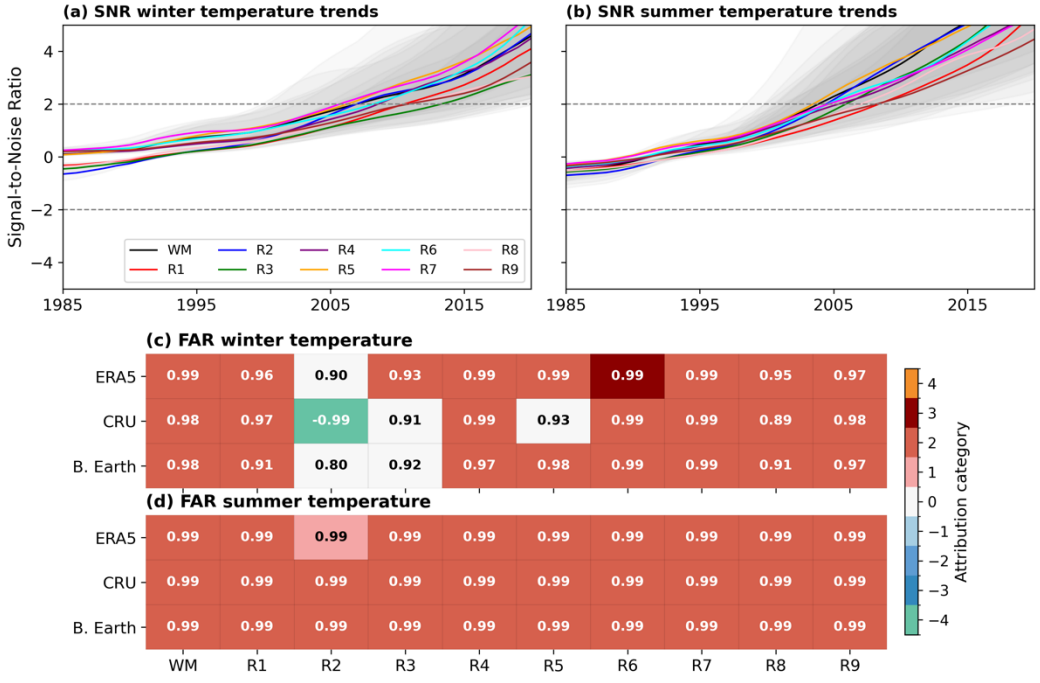

Figure 5: Detection and attribution of temperature trends over the Western Mediterranean. (a-b) Signal-to-noise ratio (SNR) as a function of trend length for (a) winter and (b) summer, based on model simulations. The horizontal dashed line indicates the emergence threshold (|SNR| = 2). (c-d) Fraction of Attributable Risk (FAR; numbers) and attribution classification categories (colours) for (c) winter and (d) summer, across sub-regions and observational datasets (ERA5, CRU, Berkeley Earth). Bold numbers indicate statistically significant differences between the Historical and Nat-only distributions based on a Kolmogorov–Smirnov test.

FAR analysis provides a quantitative estimate of the anthropogenic contribution to the observed trends (Fig. 5c-d). In both seasons, across most regions and observational datasets, FAR values exceed 0.95, indicating that anthropogenic forcing accounts for the vast majority of the probability of the observed warming trends. In summer, FAR values are consistently very high (~0.99) across all regions and datasets (Fig. 5c). In winter, slightly lower values are found in specific regions, most

https://doi.org/10.5194/egusphere-2026-2830
Preprint. Discussion started: 11 June 2026
© Author(s) 2026. CC BY 4.0 License.

notably in R2, where FAR ranges from 0.80 to 0.90 depending on the dataset, and in R3 and R5, where moderate reductions are also observed (Fig. 5d). These deviations are primarily associated with weaker or less consistent observed trends in these regions. Additionally, the Kolmogorov–Smirnov test results indicate that the distributions of trends under all forcings and natural-only forcings are statistically distinct in all regions and seasons, supporting the robustness of the FAR values obtained. The distributions of temperature trends used for these analyses are shown in Fig. S6 in the Supplement.

Overall, the three complementary approaches –SNR, categorical classification, and FAR– provide a coherent picture of robust detection and anthropogenic attribution of temperature trends across the WM, with only limited regional and seasonal deviations.

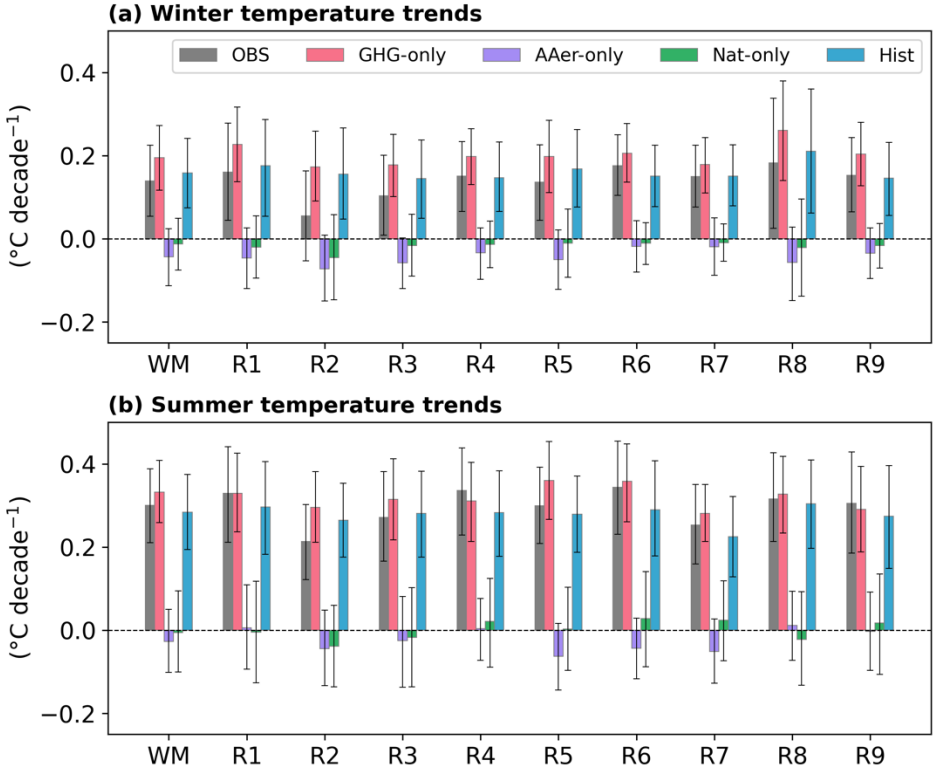

Figure 6: Estimated temperature trends for 1951-2020 across the Western Mediterranean subregions using the selected model subset for (a) winter temperature and (b) summer temperature. Bars show the best-estimate trends derived from the statistical model for observations (OBS, grey), greenhouse gas forcing only (GHG-only, pink), anthropogenic aerosols only (AAer-only, purple), and natural forcing only (Nat-only, green). Simulations with all forcings from the Historical experiments are also shown (Hist, turquoise). Best estimates correspond to $\widehat{Y}^*$ for OBS and $\widehat{Xi}^*$ for the single-forced experiments, while error bars indicate the 95% confidence intervals.

https://doi.org/10.5194/egusphere-2026-2830
Preprint. Discussion started: 11 June 2026
© Author(s) 2026. CC BY 4.0 License.

To further investigate the contribution of individual external forcings to the observed temperature trends, a statistical detection and attribution analysis based on additive decomposition and maximum likelihood estimation was applied. This framework uses the best-estimate climate responses associated with each forcing to evaluate their consistency with the observed changes.

The results indicate a dominant contribution from greenhouse gas forcing across all regions of the WM (Fig. 6). In both seasons, the trends derived from the best estimates of the greenhouse-gas response (GHG-only) are consistently positive and generally larger than the observed trends. In contrast, the trends obtained from the best estimate of the combined forcing response (Hist) are closer to the observed values, indicating that additional forcings partly offset the strong warming associated with greenhouse gases alone.

In winter, the GHG-induced warming varies across the region, with the strongest response occurring in R8 on the eastern side of the basin (+0.26 °C decade-1, 95% CI: 0.14–0.38). Anthropogenic aerosols partly compensate for this warming, producing negative trends in most regions, although these are generally not statistically significant. The strongest aerosol-induced cooling is estimated in R2 (–0.07 °C decade-1; 95% CI: –0.15 to 0.009) (Figure 6a). During summer, the GHG-induced warming is even stronger and peaks in R5 and R6 on the western side of the Western Mediterranean, with mean trends around +0.35 °C decade-1. In contrast, the aerosol-induced cooling in summer is generally weak and not statistically significant across the region, although slightly larger negative contributions appear in R5, R6, and R7 in the southwestern part of the basin (Fig. 6b). The estimated response to natural forcing remains small and not statistically distinguishable from zero across all regions and seasons, indicating a negligible contribution to the observed long-term warming.

The statistical consistency of the different forcing models is further assessed using the χ^2 test under the null hypothesis that the observed trends are consistent with the simulated forced responses (Table S2 in the Supplement). Across all regions and seasons, the model including all forcings (the sum of GHG-only, AAer-only and Nat-only) shows the highest p-values and cannot be rejected at the 5% significance level, indicating that the observed temperature trends are consistent with the combined response to external forcings. The GHG-only simulation also yields relatively high p-values in most regions, although generally lower than those of the all-forcing model, highlighting greenhouse gases as the dominant driver of the warming signal. In contrast, models including only anthropogenic aerosols, natural forcing, or internal variability show substantially lower p-values, particularly in summer, where they are frequently close to zero. These results indicate that these factors alone cannot explain the observed warming trends. The separation between forcing contributions is less pronounced in winter in some regions (e.g., R1, R2, R3, and R8), reflecting the weaker and more spatially heterogeneous winter warming signal.

https://doi.org/10.5194/egusphere-2026-2830
Preprint. Discussion started: 11 June 2026
© Author(s) 2026. CC BY 4.0 License.

3.3 Detection and attribution of precipitation trends

In contrast to temperature, precipitation trends do not emerge from internal variability across the WM. The SNR remains below the emergence threshold (|SNR| > 2) in all regions and for both seasons (Fig. 7a-b), indicating that the simulated forced signal cannot be robustly distinguished from the models' internal variability. This result is consistent with the analysis presented in Fig. 2, where precipitation trends are generally weak and statistically non-significant across most subregions. This suggests that the effect of externally forced changes in regional precipitation remains small relative to the large internal variability.

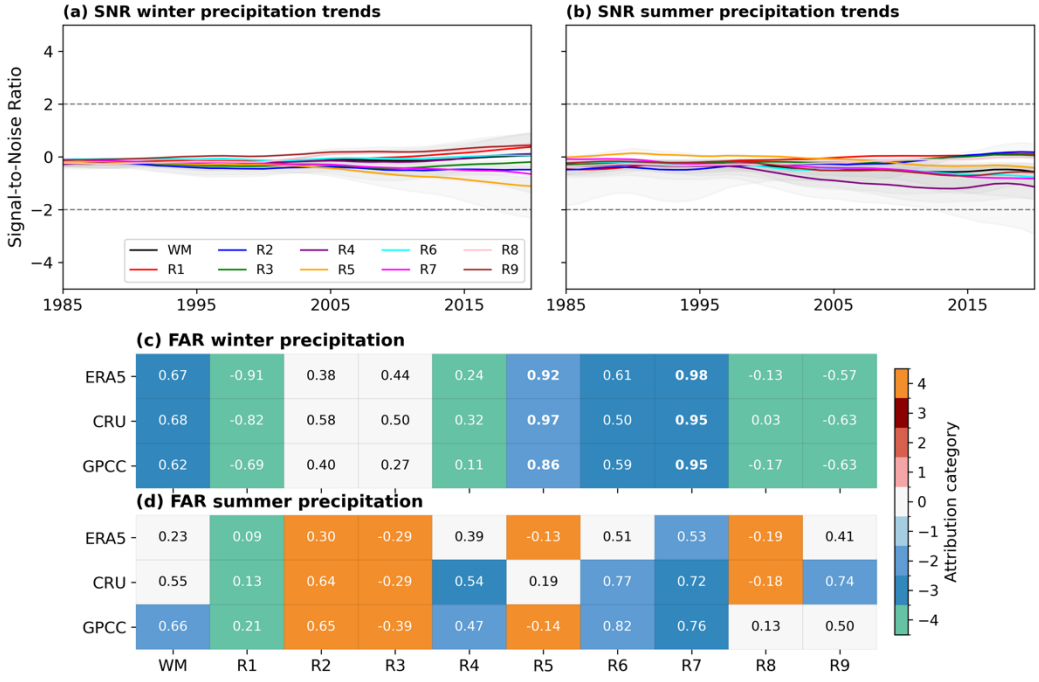

Figure 7: Detection and attribution of precipitation trends over the Western Mediterranean. (a-b) Signal-to-noise ratio (SNR) as a function of trend length for (a) winter and (b) summer, based on model simulations. The horizontal dashed line indicates the emergence threshold (|SNR| = 2). (c-d) Fraction of Attributable Risk (FAR; numbers) and attribution classification categories (colours) for (c) winter and (d) summer, across sub-regions and observational datasets (ERA5, CRU, GPCC). Bold numbers indicate statistically significant differences between the Historical and Nat-only distributions based on a Kolmogorov–Smirnov test.

The categorical classification analysis further reflects this lack of a coherent forced signal. In winter, observed trends in most regions are classified as sign-inconsistent with the model-simulated response; Category -4 is found in regions R1, R4, R8, and R9. Category -3, indicating a negative observed trend that lies outside the model-simulated range, is found for the WM as a whole as well as for R6 and R7 across the three observational datasets (Fig. 7c). In summer, the classification becomes

https://doi.org/10.5194/egusphere-2026-2830
Preprint. Discussion started: 11 June 2026
© Author(s) 2026. CC BY 4.0 License.

more diverse across regions and datasets, without a clear regional-scale pattern. For the WM as a whole, trends are classified as non-detectable in ERA5 and CRU (Category 0) and as Category -2 in GPCC (Fig. 7d), although the negative trend in GPCC is not statistically significant (Fig. 2d). Some regions show sign-inconsistent categories, such as Category -4 in R1 for all datasets and Category +4 in R2, R3, R5, and R8. Finally, statistically significant negative trends categorised as Category -2 (detectable and attributable) are limited to R5 in winter for all datasets and R6 in summer for CRU and GPCC (Fig. 2 and 7). The precipitation trend distributions used for this analysis are shown in Fig. S7 in the Supplement.

FAR results also indicate limited and regionally inconsistent attribution signals. In winter, relatively high FAR values (>0.9) are obtained in R5 and R7, suggesting a possible anthropogenic contribution to the probability of the observed trends in these regions. However, for the WM as a whole, FAR values are substantially lower (around 0.6–0.7) (Fig. 7c). In summer, FAR values are generally lower and more variable, with values around 0.5–0.8 in R6 and R7 but lower values (0.2–0.6) across most other regions and the WM as a whole (Fig. 7d). The robustness of these FAR estimates is limited: the Kolmogorov–Smirnov test indicates that in most regions, the distributions of trends under all forcings and natural-only forcings are not statistically different. This implies that even relatively high FAR values in some regions cannot be interpreted as robust evidence of attributable trends.

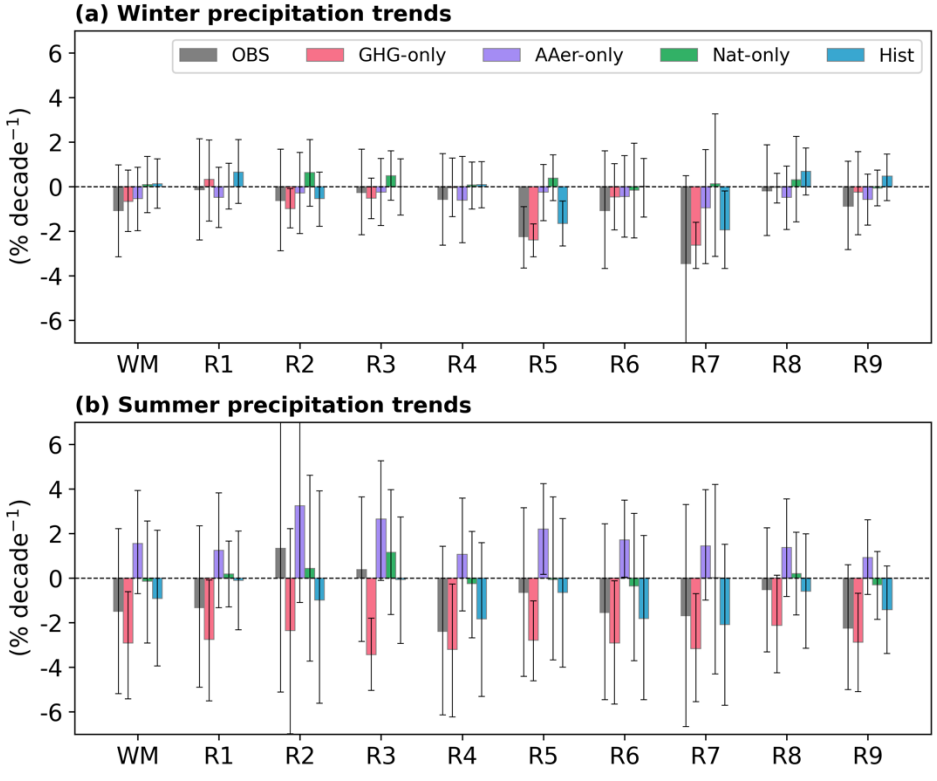

https://doi.org/10.5194/egusphere-2026-2830
Preprint. Discussion started: 11 June 2026
© Author(s) 2026. CC BY 4.0 License.

Figure 8: Estimated precipitation trends for 1951-2020 across the Western Mediterranean subregions using the selected model subset for (a) winter precipitation and (b) summer precipitation. Bars show the best-estimate trends derived from the statistical model for observations (OBS, grey), greenhouse gas forcing only (GHG-only, pink), anthropogenic aerosols only (AAer-only, purple), and natural forcing only (Nat-only, green). Simulations with all forcings from the Historical experiments are also shown (Hist, turquoise). Best estimates correspond to $\widehat{Y}^*$ for OBS and $\widehat{Xi}^*$ for the single-forced experiments, while error bars indicate the 95% confidence intervals.

The statistical attribution using the additive decomposition framework confirms that precipitation trends in the WM are largely dominated by internal variability, with very limited evidence of an externally forced signal. The observed trends (from the best estimates $\widehat{Y}^*$) are generally small and not statistically significant across regions and seasons, except for R5 in winter, where a negative trend inconsistent with zero is observed (Fig. 8). The χ^2 p-values further highlight the lack of a robust signal; only in R5 for winter, the p-values indicate that observed trends are inconsistent with internal variability (Table S3 in the Supplement). During summer, trends derived from GHG-only forcing are consistently negative and significantly different from zero in most regions, while trends associated with anthropogenic aerosols (AAer-only) are mostly positive, suggesting a potential counteracting effect between these forcings. However, given the absence of detectable signals in the observations and the large uncertainties across regions, these model-derived responses should be interpreted cautiously and primarily as an indication of the behaviour simulated by the models rather than as robust evidence of externally-forced changes in observed precipitation.

Overall, the different attribution approaches consistently indicate that precipitation trends across the WM cannot be robustly detected or attributed to anthropogenic forcings over the study period. Results remain highly heterogeneous across regions, seasons, and observational datasets, and are generally consistent with a dominant role of internal variability.

4 Discussion

The Western Mediterranean (WM) has been widely identified as one of the regions most affected by ongoing climate change, where recent temperature and precipitation trends reflect both global forcings and complex regional processes (Ali et al., 2022; Cherif et al., 2020; Jézéquel et al., 2025). Understanding the relative contribution of anthropogenic and natural drivers is therefore essential to interpret the observed changes and their implications for the region's future climate. In particular, the period since the mid-twentieth century includes a decline in winter precipitation beginning in the 1950s, whose causes remain debated between internal variability and externally forced responses (e.g., Seager et al., 2025).

In this study, seasonal temperature and precipitation trends during 1951–2020 are analysed across climatically derived sub-regions of the WM using observational datasets and a multi-method attribution framework. By combining several

https://doi.org/10.5194/egusphere-2026-2830
Preprint. Discussion started: 11 June 2026
© Author(s) 2026. CC BY 4.0 License.

complementary approaches –including the Signal-to-Noise Ratio (SNR), Fraction of Attributable Risk (FAR), distribution-based comparisons, and optimal fingerprinting– together with a performance-based selection of CMIP6 models and their Detection and Attribution (DAMIP) single-forcing experiments, this study provides a robust assessment of the drivers of recent regional climate trends.

However, both observational uncertainty and model limitations complicate the interpretation of trends in the WM. Differences between observational datasets can be substantial, particularly for precipitation and at sub-regional scales. In addition, global climate models often struggle to accurately reproduce the probability distribution of regional trends (Philip et al., 2020; Van Oldenborgh et al., 2013; Vicente-Serrano et al., 2022), before any attribution analysis, a filtering step was applied based on the spatial representation of observed trends following the regionalisation from Campos et al. (2025).

The results reveal a clear emergence of anthropogenic influence on temperature trends across the WM. The SNR analysis indicates that temperature signals exceed twice the amplitude of internal variability ($|SNR| > 2$) in all sub-regions, suggesting that the forced signal has robustly emerged from the background noise of natural variability. The FAR analysis further supports this result, showing that anthropogenic forcings account for more than 95% of the probability of the observed warming in most regions during summer, with similarly high contributions in winter. Comparable attribution results have been reported at broader spatial scales, where anthropogenic forcing has been shown to dominate observed warming trends across Europe and the Mediterranean basin (e.g., Feng et al., 2022; Stott, 2003).

The analysis of single-forcing simulations indicates that greenhouse gas (GHG) emissions are the dominant driver of the observed warming, especially in summer. In contrast, anthropogenic aerosols (AAer) exert a cooling influence that partially offsets the GHG-induced warming. This behaviour is consistent with the historical evolution of aerosol emissions during the second half of the twentieth century. The cooling effect associated with aerosols during the so-called “global dimming” period (approximately 1950–1980; Wild, 2012) has been documented over Europe and the Mediterranean (Nabat et al., 2014; Pfeifroth et al., 2018), however the spatial pattern of the aerosol response is not uniform across the WM, with a stronger and more homogeneous cooling signal in winter, while in summer the influence is more pronounced over the southwestern sub-regions. An exploratory analysis of the period 1981-2020 suggest a shift in the aerosol response to warming (not shown), as a result of the reduction in aerosol emissions since the 1980s (Floutsi et al., 2016; J. Li et al., 2014) has led to a “brightening” phase that has contributed to the accelerated warming observed in recent decades (Glantz et al., 2022; Urdiales-Flores et al., 2023).

In contrast to temperature, precipitation trends across the WM remain largely within the bounds of internal variability. The SNR analysis shows that precipitation signals have not yet emerged from the models’ internal variability in all sub-regions. This limited detectability is consistent with the observational analysis, which shows that precipitation trends are generally

https://doi.org/10.5194/egusphere-2026-2830
Preprint. Discussion started: 11 June 2026
© Author(s) 2026. CC BY 4.0 License.

weak and statistically non-significant across most subregions. Although some regions in the southern and southwestern WM display signals approaching detectability, particularly in northern Africa (R5), the overall results indicate that externally forced precipitation changes remain difficult to identify in observations. These findings are consistent with previous studies highlighting the strong role of internal variability in shaping Mediterranean precipitation trends in recent decades (e.g., Campos et al., 2025; Seager et al., 2025; Vicente-Serrano et al., 2022), despite consistent model projections indicating a drying signal emerging in the future (Cos et al., 2022a; Giorgi & Bi, 2009; Mariotti et al., 2008, 2015; Olmo et al., 2025; Seager et al., 2024).

In addition, the additive decomposition framework indicates that internal variability cannot be rejected as an explanation for the observed precipitation trends across most regions and seasons. Only in northern Africa (R5) during winter does the analysis suggest that the observed trend is inconsistent with internal variability; however, as discussed above, observational constraints in this region remain limited, with fewer available station records and reduced consistency across datasets, which calls for caution in the interpretation of this regional signal. Model-derived responses nevertheless provide insight into how different forcings may influence regional precipitation. Simulations driven by GHG produce negative precipitation trends in the southeastern regions (R5 and R7) during winter. During summer, the simulated responses reveal a contrasting behaviour between external forcings: while GHG forcing tends to produce drying, AAer are associated with weak positive precipitation trends, suggesting a partial counteracting effect between these forcings. A similar contrast between GHG-induced drying and aerosol-related moistening has also been reported in projections of future Mediterranean precipitation (Wang et al., 2023). However, given that internal variability cannot be rejected as the primary explanation for the observed trends, these simulated responses cannot be interpreted as robust explanations of the observed precipitation behaviour.

The use of multiple detection and attribution approaches provides complementary perspectives on the drivers of recent climate trends in the WM. Each method captures different aspects of the attribution problem and therefore helps strengthen the robustness of the overall conclusions. The convergence of independent methods for temperature –all indicating a robust anthropogenic signal dominated by greenhouse gas forcing– increases confidence in the attribution results. In contrast, for precipitation, the different approaches consistently reinforce the interpretation that internal variability remains the dominant driver of observed trends.

At the same time, several limitations should be acknowledged. All approaches rely on climate model simulations to estimate both the forced response and internal variability, implying that potential model biases or structural uncertainties may influence the attribution results. In addition, assumptions such as the additivity of forcing responses or the representativeness of pre-industrial control simulations for estimating internal variability may not fully capture the complexity of regional hydroclimate dynamics. The regional analysis adopted here –necessary to represent the pronounced climatic heterogeneity of the WM, where multiple dynamical processes influence temperature and precipitation variability (Olmo et al., 2024)– also

https://doi.org/10.5194/egusphere-2026-2830
Preprint. Discussion started: 11 June 2026
© Author(s) 2026. CC BY 4.0 License.

poses challenges for global climate models, which still operate at relatively coarse spatial resolutions. The subset of models used for the detection and attribution analysis was selected based on their ability to reproduce the observed spatial contrasts in trends across subregions, rather than their capacity to match the exact magnitude of observed trends within each individual region. This filtering aimed to retain models that capture the regional heterogeneity of the WM climate response. Sensitivity analyses performed without this model selection yield qualitatively similar results for both temperature and precipitation (not shown), although with increased noise, particularly for precipitation in the southwestern subregions, where observational datasets show relatively coherent signals.

Observational limitations represent an additional source of uncertainty (González-Hidalgo & Vicente-Serrano, 2025; Vicente-Serrano et al., 2025). The network of ground stations fully available for comparison is relatively sparse and unevenly distributed across the region, limiting the ability to fully assess the robustness of spatial patterns derived from gridded datasets, which do not always agree in the magnitude or spatial distribution of temperature and precipitation trends across the WM.

Future work should also further investigate other aspects of sub-regional climate change in the WM, particularly the behaviour of extreme events under continued global warming and their links to changes in atmospheric dynamics and physical processes. Such analyses would help to provide a more comprehensive understanding of the mechanisms driving regional climate responses.

5 Conclusions

This study assessed the detection and attribution of seasonal temperature and precipitation trends during 1951-2020 across climatically derived subregions of the Western Mediterranean using a multi-method framework and CMIP6 DAMIP single-forcing experiments. Results reveal a robust anthropogenic influence on temperature across all regions, with forced signals clearly emerging from internal variability. Greenhouse gas emissions are identified as the dominant driver of the observed warming, while anthropogenic aerosols exert a cooling influence that partially offsets the greenhouse gas-induced warming. The strongest greenhouse-gas-driven warming is simulated in summer over the southwestern subregions, while slightly weaker and more heterogeneous signals occur in some northern regions during winter.

In contrast, precipitation trends across the Western Mediterranean remain largely consistent with internal variability over the study period. None of the attribution approaches provide robust evidence of externally forced precipitation changes across most regions and seasons, despite model simulations indicating potential drying responses to greenhouse gas forcing in some areas. Only northern Africa in winter shows signals approaching detectability, although observational limitations in this region introduce substantial uncertainty. These results highlight the contrasting detectability of temperature and precipitation

https://doi.org/10.5194/egusphere-2026-2830
Preprint. Discussion started: 11 June 2026
© Author(s) 2026. CC BY 4.0 License.

responses to external forcing in the region and underline the importance of regional-scale attribution frameworks and careful model evaluation for improving the understanding of Mediterranean climate change.

Code availability

All the Jupyter Notebooks and codes used for the analysis will be available in a GitHub repository after acceptance.

Data availability

Monthly ERA5 data is available from the Copernicus Climate Change Service (Copernicus Climate Change Service, 2019). CRU monthly temperature and precipitation data are available from the Climatic Research Unit webpage (https://crudata.uea.ac.uk/cru/data/hrg/#info), Berkeley Earth monthly temperature is available from the Berkeley Earth data webpage (https://berkeleyearth.org/data/), GPCC monthly precipitation data is available from the DWD webpage (https://www.dwd.de/EN/ourservices/gpcc/gpcc.html). The CMIP6-DAMIP model outputs used in this study are available online in https://esgf-node.llnl.gov/search /cmip6/.

Daily temperature and precipitation data from the European Climate Assessment & Dataset (ECA&D) is available via the ECA&D webpage (https://www.ecad.eu/dailydata/index.php). Daily temperature and precipitation data from the Daily Global Historical Climatology Network (GHCN-Daily), Version 3 are available via the NOAA-NCEI Direct Download access (https://www.ncei.noaa.gov/data/global-historical-climatology-network-daily/).

Author contributions

DC, MO, and FDR designed the study. DC developed the diagnostics and analyses and wrote the initial manuscript. MS downloaded and organised the data. DC, MO, PC, and FDR contributed to the interpretation and discussion of the results.

Competing interests

The authors declare that they have no conflict of interest.

Financial support

MO is funded by the AI4Science PN070500 fellowship within the “Generación D” initiative, Red.es, Ministerio para la Transformación Digital y de la Función Pública, for talent attraction (C005/24-ED CV1). Funded by the European Union NextGenerationEU funds, through PRTR. FJDR has been supported by the Horizon Europe ASPECT project (grant no. 101081460).

https://doi.org/10.5194/egusphere-2026-2830
Preprint. Discussion started: 11 June 2026
© Author(s) 2026. CC BY 4.0 License.

References

Ali, E., Cramer, W., Carnicer, J., Georgopoulou, E., Hilmi, N., Le Cozannet, G., & Lionello, P. (2022). Cross-Chapter Paper 4: Mediterranean Region. In Climate Change 2022: Impacts, Adaptation and Vulnerability. Contribution of Working Group II to the Sixth Assessment Report of the Intergovernmental Panel on Climate Change (pp. 2233–2272). Cambridge University Press.

Allen, M. R., & Stott, P. A. (2003). Estimating signal amplitudes in optimal fingerprinting, part I: Theory. Climate Dynamics, 21(5–6), 477–491. https://doi.org/10.1007/s00382-003-0313-9

Andrews, M. B., Ridley, J. K., Wood, R. A., Andrews, T., Blockley, E. W., Booth, B., Burke, E., Dittus, A. J., Florek, P., Gray, L. J., Haddad, S., Hardiman, S. C., Hermanson, L., Hodson, D., Hogan, E., Jones, G. S., Knight, J. R., Kuhlbrodt, T., Misios, S., … Sutton, R. T. (2020). Historical Simulations With HadGEM3-GC3.1 for CMIP6. Journal of Advances in Modeling Earth Systems, 12(6), e2019MS001995. https://doi.org/10.1029/2019MS001995

Bentsen, M., Bethke, I., Debernard, J. B., Iversen, T., Kirkevåg, A., Seland, Ø., Drange, H., Roelandt, C., Seierstad, I. A., Hoose, C., & Kristjánsson, J. E. (2013). The Norwegian Earth System Model, NorESM1-M – Part 1: Description and basic evaluation of the physical climate. Geoscientific Model Development, 6(3), 687–720. https://doi.org/10.5194/gmd-6-687-2013

Boucher, O., Servonnat, J., Albright, A. L., Aumont, O., Balkanski, Y., Bastrikov, V., Bekki, S., Bonnet, R., Bony, S., Bopp, L., Braconnot, P., Brockmann, P., Cadule, P., Caubel, A., Cheruy, F., Codron, F., Cozic, A., Cugnet, D., D'Andrea, F., … Vuichard, N. (2020). Presentation and Evaluation of the IPSL-CM6A-LR Climate Model. Journal of Advances in Modeling Earth Systems, 12(7), e2019MS002010. https://doi.org/10.1029/2019MS002010

Campos, D. A., Olmo, M. E., Cos, P., Muñoz, Á. G., & Doblas-Reyes, F. J. (2025). Regional Aspects of Observed Temperature and Precipitation Trends in the Western Mediterranean: Insights From a Timescale Decomposition Analysis. Journal of Geophysical Research: Atmospheres, 130(19), e2024JD042637. https://doi.org/10.1029/2024JD042637

Carvalho, D., Pereira, S. C., Silva, R., & Rocha, A. (2022). Aridity and desertification in the Mediterranean under EURO-CORDEX future climate change scenarios. Climatic Change, 174(3–4), 28. https://doi.org/10.1007/s10584-022-03454-4

Chemke, R., & Coumou, D. (2024). Human influence on the recent weakening of storm tracks in boreal summer. Npj Climate and Atmospheric Science, 7(1), 86. https://doi.org/10.1038/s41612-024-00640-2

Cherif, S., Doblas-Miranda, E., Lionello, P., Borrego, C., Giorgi, F., Iglesias, A., Jebari, S., Mahmoudi, E., Moriondo, M., Pringault, O., Rilov, G., Somot, S., Tsikliras, A., Vilà, M., & Zittis, G. (2020). Drivers of Change. In W. Cramer, J. Guiot, & K. Marini (Eds.), Climate and Enviromental Change in the Mediterranean Basin—Current Situation and Risks for the Future (pp. 59–180). Union for the Mediterranean, Plan Bleu, UNEP/MAP.

Christidis, N., & Stott, P. A. (2021). The influence of anthropogenic climate change on wet and dry summers in Europe. Science Bulletin, 66(8), 813–823. https://doi.org/10.1016/j.scib.2021.01.020

https://doi.org/10.5194/egusphere-2026-2830
Preprint. Discussion started: 11 June 2026
© Author(s) 2026. CC BY 4.0 License.

Christidis, N., & Stott, P. A. (2022). Human Influence on Seasonal Precipitation in Europe. Journal of Climate, 35(15), 5215–5231. https://doi.org/10.1175/JCLI-D-21-0637.1

Cos, J., Doblas-Reyes, F., Jury, M., Marcos, R., Bretonnière, P.-A., & Samsó, M. (2022a). The Mediterranean climate change hotspot in the CMIP5 and CMIP6 projections. Earth Syst. Dynam., 13(1), 321–340. https://doi.org/10.5194/esd-13-321-2022

Cos, J., Doblas-Reyes, F., Jury, M., Marcos, R., Bretonnière, P.-A., & Samsó, M. (2022b). The Mediterranean climate change hotspot in the CMIP5 and CMIP6 projections. Earth System Dynamics, 13(1), 321–340. https://doi.org/10.5194/esd-13-321-2022

Cramer, W., Guiot, J., Fader, M., Garrabou, J., Gattuso, J.-P., Iglesias, A., Lange, M. A., Lionello, P., Llasat, M. C., Paz, S., Peñuelas, J., Snoussi, M., Toreti, A., Tsimplis, M. N., & Xoplaki, E. (2018). Climate change and interconnected risks to sustainable development in the Mediterranean. Nature Climate Change, 8(11), 972–980. https://doi.org/10.1038/s41558-018-0299-2

De Abreu, R. C., Tett, S. F. B., Schurer, A., & Rocha, H. R. (2019). Attribution of Detected Temperature Trends in Southeast Brazil. Geophysical Research Letters, 46(14), 8407–8414. https://doi.org/10.1029/2019GL083003

Donat, M. G., Delgado-Torres, C., De Luca, P., Mahmood, R., Ortega, P., & Doblas-Reyes, F. J. (2023). How Credibly Do CMIP6 Simulations Capture Historical Mean and Extreme Precipitation Changes? Geophysical Research Letters, 50(14), e2022GL102466. https://doi.org/10.1029/2022GL102466

Driouech, F., ElRhaz, K., Moufouma-Okia, W., Arjdal, K., & Balhane, S. (2020). Assessing Future Changes of Climate Extreme Events in the CORDEX-MENA Region Using Regional Climate Model ALADIN-Climate. Earth Systems and Environment, 4(3), 477–492. https://doi.org/10.1007/s41748-020-00169-3

Eyring, V., Bony, S., Meehl, G. A., Senior, C. A., Stevens, B., Stouffer, R. J., & Taylor, K. E. (2016). Overview of the Coupled Model Intercomparison Project Phase 6 (CMIP6) experimental design and organization. Geoscientific Model Development, 9(5), 1937–1958. https://doi.org/10.5194/gmd-9-1937-2016

Feng, X., Qian, C., & Materia, S. (2022). Amplification of the Temperature Seasonality in the Mediterranean Region Under Anthropogenic Climate Change. Geophysical Research Letters, 49(20), e2022GL099658. https://doi.org/10.1029/2022GL099658

Floutsi, A. A., Korras-Carraca, M. B., Matsoukas, C., Hatzianastassiou, N., & Biskos, G. (2016). Climatology and trends of aerosol optical depth over the Mediterranean basin during the last 12 years (2002–2014) based on Collection 006 MODIS-Aqua data. Science of The Total Environment, 551–552, 292–303. https://doi.org/10.1016/j.scitotenv.2016.01.192

Gillett, N. P., Shiogama, H., Funke, B., Hegerl, G., Knutti, R., Matthes, K., Santer, B. D., Stone, D., & Tebaldi, C. (2016). The Detection and Attribution Model Intercomparison Project (DAMIP v1.0)contribution to CMIP6. Geoscientific Model Development, 9(10), 3685–3697. https://doi.org/10.5194/gmd-9-3685-2016

Giorgi, F., & Bi, X. (2009). Time of emergence (TOE) of GHG-forced precipitation change hot-spots. Geophysical Research Letters, 36(6), 2009GL037593. https://doi.org/10.1029/2009GL037593

https://doi.org/10.5194/egusphere-2026-2830
Preprint. Discussion started: 11 June 2026
© Author(s) 2026. CC BY 4.0 License.

Giorgi, F., & Lionello, P. (2008). Climate change projections for the Mediterranean region. Global and Planetary Change, 63(2–3), 90–104. https://doi.org/10.1016/j.gloplacha.2007.09.005

Glantz, P., Fawole, O. G., Ström, J., Wild, M., & Noone, K. J. (2022). Unmasking the Effects of Aerosols on Greenhouse Warming Over Europe. Journal of Geophysical Research: Atmospheres, 127(22), e2021JD035889. https://doi.org/10.1029/2021JD035889

González-Hidalgo, J. C., & Vicente-Serrano, S. M. (2025). Is There a Precipitation Decline in the Mediterranean Region? An Assessment Based on the Scientific Literatured. International Journal of Climatology, 45(9), e8918. https://doi.org/10.1002/joc.8918

Harris, I., Osborn, T. J., Jones, P., & Lister, D. (2020). Version 4 of the CRU TS monthly high-resolution gridded multivariate climate dataset. Scientific Data, 7(1), 109. https://doi.org/10.1038/s41597-020-0453-3

Hawkins, E., & Sutton, R. (2012). Time of emergence of climate signals. Geophysical Research Letters, 39(1), 2011GL050087. https://doi.org/10.1029/2011GL050087

Hegerl, G., Zwiers, F., & Tebaldi, C. (2011). Patterns of change: Whose fingerprint is seen in global warming? Environmental Research Letters, 6(4), 044025. https://doi.org/10.1088/1748-9326/6/4/044025

Hersbach, H., Bell, B., Berrisford, P., Hirahara, S., Horányi, A., Muñoz-Sabater, J., Nicolas, J., Peubey, C., Radu, R., Schepers, D., Simmons, A., Soci, C., Abdalla, S., Abellan, X., Balsamo, G., Bechtold, P., Biavati, G., Bidlot, J., Bonavita, M., … Thépaut, J. (2020). The ERA5 global reanalysis. Quarterly Journal of the Royal Meteorological Society, 146(730), 1999–2049. https://doi.org/10.1002/qj.3803

Hoerling, M., Eischeid, J., Perlwitz, J., Quan, X., Zhang, T., & Pegion, P. (2012). On the Increased Frequency of Mediterranean Drought. Journal of Climate, 25(6), 2146–2161. https://doi.org/10.1175/JCLI-D-11-00296.1

IPCC. (2022). Climate Change 2022 – Impacts, Adaptation and Vulnerability: Working Group II Contribution to the Sixth Assessment Report of the Intergovernmental Panel on Climate Change (1st ed.). Cambridge University Press. https://doi.org/10.1017/9781009325844

Jézéquel, A., Faranda, D., Drobinski, P., & Lionello, P. (2025). Extreme Event Attribution in the Mediterranean. International Journal of Climatology, 45(7), e8799. https://doi.org/10.1002/joc.8799

Klein Tank, A. M. G., Wijngaard, J. B., Können, G. P., Böhm, R., Demarée, G., Gocheva, A., Mileta, M., Pashiardis, S., Hejkrlik, L., Kern-Hansen, C., Heino, R., Bessemoulin, P., Müller-Westermeier, G., Tzanakou, M., Szalai, S., Pálsdóttir, T., Fitzgerald, D., Rubin, S., Capaldo, M., … Petrovic, P. (2002). Daily dataset of 20th-century surface air temperature and precipitation series for the European Climate Assessment. International Journal of Climatology, 22(12), 1441–1453. https://doi.org/10.1002/joc.773

Knutson, T. R., & Zeng, F. (2018). Model Assessment of Observed Precipitation Trends over Land Regions: Detectable Human Influences and Possible Low Bias in Model Trends. Journal of Climate, 31(12), 4617–4637. https://doi.org/10.1175/JCLI-D-17-0672.1

https://doi.org/10.5194/egusphere-2026-2830
Preprint. Discussion started: 11 June 2026
© Author(s) 2026. CC BY 4.0 License.

Li, J., Carlson, B. E., Dubovik, O., & Lacis, A. A. (2014). Recent trends in aerosol optical properties derived from AERONET measurements. Atmospheric Chemistry and Physics, 14(22), 12271–12289. https://doi.org/10.5194/acp-14-12271-2014

Li, L., Yu, Y., Tang, Y., Lin, P., Xie, J., Song, M., Dong, L., Zhou, T., Liu, L., Wang, L., Pu, Y., Chen, X., Chen, L., Xie, Z., Liu, H., Zhang, L., Huang, X., Feng, T., Zheng, W., … Wei, J. (2020). The Flexible Global Ocean-Atmosphere-Land System Model Grid-Point Version 3 (FGOALS-g3): Description and Evaluation. Journal of Advances in Modeling Earth Systems, 12(9), e2019MS002012. https://doi.org/10.1029/2019MS002012

Lionello, P., Abrantes, F., Congedi, L., Dulac, F., Gacic, M., Gomis, D., Goodess, C., Hoff, H., Kutiel, H., Luterbacher, J., Planton, S., Reale, M., Schröder, K., Vittoria Struglia, M., Toreti, A., Tsimplis, M., Ulbrich, U., & Xoplaki, E. (2012). Introduction: Mediterranean Climate—Background Information. In The Climate of the Mediterranean Region (pp. xxxv–xc). Elsevier. https://doi.org/10.1016/B978-0-12-416042-2.00012-4

Mann, H. B., & Whitney, D. R. (1947). On a Test of Whether one of Two Random Variables is Stochastically Larger than the Other. The Annals of Mathematical Statistics, 18(1), 50–60.

Mariotti, A., Pan, Y., Zeng, N., & Alessandri, A. (2015). Long-term climate change in the Mediterranean region in the midst of decadal variability. Climate Dynamics, 44(5–6), 1437–1456. https://doi.org/10.1007/s00382-015-2487-3

Mariotti, A., Zeng, N., Yoon, J.-H., Artale, V., Navarra, A., Alpert, P., & Li, L. Z. X. (2008). Mediterranean water cycle changes: Transition to drier 21st century conditions in observations and CMIP3 simulations. Environmental Research Letters, 3(4), 044001. https://doi.org/10.1088/1748-9326/3/4/044001

McSweeney, C. F., Jones, R. G., Lee, R. W., & Rowell, D. P. (2015). Selecting CMIP5 GCMs for downscaling over multiple regions. Climate Dynamics, 44(11–12), 3237–3260. https://doi.org/10.1007/s00382-014-2418-8

Menne, M. J., Durre, I., Vose, R. S., Gleason, B. E., & Houston, T. G. (2012). An Overview of the Global Historical Climatology Network-Daily Database. Journal of Atmospheric and Oceanic Technology, 29(7), 897–910. https://doi.org/10.1175/JTECH-D-11-00103.1

Merrifield, A. L., Brunner, L., Lorenz, R., Humphrey, V., & Knutti, R. (2023). Climate model Selection by Independence, Performance, and Spread (ClimSIPS v1.0.1) for regional applications. Geoscientific Model Development, 16(16), 4715–4747. https://doi.org/10.5194/gmd-16-4715-2023

Nabat, P., Somot, S., Mallet, M., Sanchez-Lorenzo, A., & Wild, M. (2014). Contribution of anthropogenic sulfate aerosols to the changing Euro-Mediterranean climate since 1980. Geophysical Research Letters, 41(15), 5605–5611. https://doi.org/10.1002/2014GL060798

Olmo, M., Cos, P., Muñoz, Á. G., Altava-Ortiz, V., Barrera-Escoda, A., Campos, D., Soret, A., & Doblas-Reyes, F. (2024). Cross-time scale analysis of year-round atmospheric circulation patterns and their impacts on rainfall and temperatures in the Iberian Peninsula. Journal of Climate. https://doi.org/10.1175/JCLI-D-23-0735.1

https://doi.org/10.5194/egusphere-2026-2830
Preprint. Discussion started: 11 June 2026
© Author(s) 2026. CC BY 4.0 License.

Olmo, M. E., Cos, P., Campos, D., Muñoz, A. G., Altava-Ortiz, V., Barrera-Escoda, A., Jury, M., Loosveldt-Tomas, S., Bretonniere, P. A., Doblas-Reyes, F., & Soret, A. (2025). Filtering CMIP6 models in the Euro-Mediterranean based on a circulation patterns approach. Weather and Climate Extremes, 100765. https://doi.org/10.1016/j.wace.2025.100765

Palmer, T. E., McSweeney, C. F., Booth, B. B. B., Priestley, M. D. K., Davini, P., Brunner, L., Borchert, L., & Menary, M. B. (2023). Performance-based sub-selection of CMIP6 models for impact assessments in Europe. Earth System Dynamics, 14(2), 457–483. https://doi.org/10.5194/esd-14-457-2023

Peña-Angulo, D., Vicente-Serrano, S. M., Domínguez-Castro, F., Murphy, C., Reig, F., Tramblay, Y., Trigo, R. M., Luna, M. Y., Turco, M., Noguera, I., Aznárez-Balta, M., García-Herrera, R., Tomas-Burguera, M., & El Kenawy, A. (2020). Long-term precipitation in Southwestern Europe reveals no clear trend attributable to anthropogenic forcing. Environmental Research Letters, 15(9), 094070. https://doi.org/10.1088/1748-9326/ab9c4f

Pfeifroth, U., Sanchez-Lorenzo, A., Manara, V., Trentmann, J., & Hollmann, R. (2018). Trends and Variability of Surface Solar Radiation in Europe Based On Surface- and Satellite-Based Data Records. Journal of Geophysical Research: Atmospheres, 123(3), 1735–1754. https://doi.org/10.1002/2017JD027418

Philip, S., Kew, S., Van Oldenborgh, G. J., Otto, F., Vautard, R., Van Der Wiel, K., King, A., Lott, F., Arrighi, J., Singh, R., & Van Aalst, M. (2020). A protocol for probabilistic extreme event attribution analyses. Advances in Statistical Climatology, Meteorology and Oceanography, 6(2), 177–203. https://doi.org/10.5194/ascmo-6-177-2020

Philipona, R., Behrens, K., & Ruckstuhl, C. (2009). How declining aerosols and rising greenhouse gases forced rapid warming in Europe since the 1980s. Geophysical Research Letters, 36(2), 2008GL036350. https://doi.org/10.1029/2008GL036350

Riahi, K., Van Vuuren, D. P., Kriegler, E., Edmonds, J., O'Neill, B. C., Fujimori, S., Bauer, N., Calvin, K., Dellink, R., Fricko, O., Lutz, W., Popp, A., Cuaresma, J. C., Kc, S., Leimbach, M., Jiang, L., Kram, T., Rao, S., Emmerling, J., … Tavoni, M. (2017). The Shared Socioeconomic Pathways and their energy, land use, and greenhouse gas emissions implications: An overview. Global Environmental Change, 42, 153–168. https://doi.org/10.1016/j.gloenvcha.2016.05.009

Ribes, A., Planton, S., & Terray, L. (2013). Application of regularised optimal fingerprinting to attribution. Part I: Method, properties and idealised analysis. Climate Dynamics, 41(11–12), 2817–2836. https://doi.org/10.1007/s00382-013-1735-7

Ribes, A., & Terray, L. (2013). Application of regularised optimal fingerprinting to attribution. Part II: Application to global near-surface temperature. Climate Dynamics, 41(11–12), 2837–2853. https://doi.org/10.1007/s00382-013-1736-6

Ribes, A., Zwiers, F. W., Azaïs, J.-M., & Naveau, P. (2017). A new statistical approach to climate change detection and attribution. Climate Dynamics, 48(1–2), 367–386. https://doi.org/10.1007/s00382-016-3079-6

Righi, M., Andela, B., Eyring, V., Lauer, A., Predoi, V., Schlund, M., Vegas-Regidor, J., Bock, L., Brötz, B., De Mora, L., Diblen, F., Dreyer, L., Drost, N., Earnshaw, P., Hassler, B., Koldunov, N., Little, B., Loosveldt Tomas, S., & Zimmermann, K. (2020). Earth System Model Evaluation Tool (ESMValTool) v2.0 – technical overview. Geoscientific Model Development, 13(3), 1179–1199. https://doi.org/10.5194/gmd-13-1179-2020

https://doi.org/10.5194/egusphere-2026-2830
Preprint. Discussion started: 11 June 2026
© Author(s) 2026. CC BY 4.0 License.

Rohde, R. A., & Hausfather, Z. (2020). The Berkeley Earth Land/Ocean Temperature Record. Earth System Science Data, 12(4), 3469–3479. https://doi.org/10.5194/essd-12-3469-2020

Schneider, U., Hänsel, S., Finger, P., Rustemeier, E., & Ziese, M. (2022). GPCC Climatology Version 2022 at 0.25°: Monthly Land-Surface Precipitation Climatology for Every Month and the Total Year from Rain-Gauges built on GTS-based and Historical Data: Globally Gridded Monthly Totals (Version 2022, p. min. 200 KByte-max. 10 MByte per gzip archive) [NetCDF]. Global Precipitation Climatology Centre at Deutscher Wetterdienst. https://doi.org/10.5676/DWD_GPCC/CLIM_M_V2022_025

Schumacher, D. L., Singh, J., Hauser, M., Fischer, E. M., Wild, M., & Seneviratne, S. I. (2024). Exacerbated summer European warming not captured by climate models neglecting long-term aerosol changes. Communications Earth & Environment, 5(1), 182. https://doi.org/10.1038/s43247-024-01332-8

Seager, R., Liu, H., Henderson, N., Simpson, I., Kelley, C., Shaw, T., Kushnir, Y., & Ting, M. (2014). Causes of Increasing Aridification of the Mediterranean Region in Response to Rising Greenhouse Gases*. Journal of Climate, 27(12), 4655–4676. https://doi.org/10.1175/JCLI-D-13-00446.1

Seager, R., Liu, H., Osborn, Tim. J., Kushnir, Y., Nakamura, J., & Wu, Y. (2025). Mediterranean drying by a positive North Atlantic Oscillation trend over the last 65 years is an extreme outlier in the CMIP6 multimodel ensemble. Journal of Climate, e250359. https://doi.org/10.1175/JCLI-D-25-0359.1

Seager, R., Wu, Y., Cherchi, A., Simpson, I. R., Osborn, T. J., Kushnir, Y., Lukovic, J., Liu, H., & Nakamura, J. (2024). Recent and near-term future changes in impacts-relevant seasonal hydroclimate in the world's Mediterranean climate regions. International Journal of Climatology, 44(11), 3792–3820. https://doi.org/10.1002/joc.8551

Stott, P. A. (2003). Attribution of regional-scale temperature changes to anthropogenic and natural causes. Geophysical Research Letters, 30(14), 2003GL017324. https://doi.org/10.1029/2003GL017324

Stott, P. A., Christidis, N., Otto, F. E. L., Sun, Y., Vanderlinden, J., Van Oldenborgh, G. J., Vautard, R., Von Storch, H., Walton, P., Yiou, P., & Zwiers, F. W. (2016). Attribution of extreme weather and climate-related events. WIREs Climate Change, 7(1), 23–41. https://doi.org/10.1002/wcc.380

Swart, N. C., Cole, J. N. S., Kharin, V. V., Lazare, M., Scinocca, J. F., Gillett, N. P., Anstey, J., Arora, V., Christian, J. R., Hanna, S., Jiao, Y., Lee, W. G., Majaess, F., Saenko, O. A., Seiler, C., Seinen, C., Shao, A., Sigmond, M., Solheim, L., … Winter, B. (2019). The Canadian Earth System Model version 5 (CanESM5.0.3). Geoscientific Model Development, 12(11), 4823–4873. https://doi.org/10.5194/gmd-12-4823-2019

Tarín-Carrasco, P., Petrova, D., Chica-Castells, L., Lukovic, J., Rodó, X., & Cvijanovic, I. (2025). Assessment of Future Precipitation Changes in Mediterranean Climate Regions From CMIP6 Ensemble. International Journal of Climatology, 45(12), e70039. https://doi.org/10.1002/joc.70039

Tatebe, H., Ogura, T., Nitta, T., Komuro, Y., Ogochi, K., Takemura, T., Sudo, K., Sekiguchi, M., Abe, M., Saito, F., Chikira, M., Watanabe, S., Mori, M., Hirota, N., Kawatani, Y., Mochizuki, T., Yoshimura, K., Takata, K., O'ishi, R., … Kimoto, M.

https://doi.org/10.5194/egusphere-2026-2830
Preprint. Discussion started: 11 June 2026
© Author(s) 2026. CC BY 4.0 License.

(2019). Description and basic evaluation of simulated mean state, internal variability, and climate sensitivity in MIROC6. Geoscientific Model Development, 12(7), 2727–2765. https://doi.org/10.5194/gmd-12-2727-2019

Taylor, K. E. (2001). Summarizing multiple aspects of model performance in a single diagram. Journal of Geophysical Research: Atmospheres, 106(D7), 7183–7192. https://doi.org/10.1029/2000JD900719

Tuel, A., & Eltahir, E. A. B. (2020). Why Is the Mediterranean a Climate Change Hot Spot? JOURNAL OF CLIMATE, 33.

Urdiales-Flores, D., Zittis, G., Hadjinicolaou, P., Osipov, S., Klingmüller, K., Mihalopoulos, N., Kanakidou, M., Economou, T., & Lelieveld, J. (2023). Drivers of accelerated warming in Mediterranean climate-type regions. Npj Climate and Atmospheric Science, 6(1), 97. https://doi.org/10.1038/s41612-023-00423-1

Van Oldenborgh, G. J., Doblas Reyes, F. J., Drijfhout, S. S., & Hawkins, E. (2013). Reliability of regional climate model trends. Environmental Research Letters, 8(1), 014055. https://doi.org/10.1088/1748-9326/8/1/014055

Van Oldenborgh, G. J., Drijfhout, S., Van Ulden, A., Haarsma, R., Sterl, A., Severijns, C., Hazeleger, W., & Dijkstra, H. (2009). Western Europe is warming much faster than expected. Climate of the Past, 5(1), 1–12. https://doi.org/10.5194/cp-5-1-2009

Vicente-Serrano, S. M., García-Herrera, R., Peña-Angulo, D., Tomas-Burguera, M., Domínguez-Castro, F., Noguera, I., Calvo, N., Murphy, C., Nieto, R., Gimeno, L., Gutierrez, J. M., Azorin-Molina, C., & El Kenawy, A. (2022). Do CMIP models capture long-term observed annual precipitation trends? Climate Dynamics, 58(9–10), 2825–2842. https://doi.org/10.1007/s00382-021-06034-x

Vicente-Serrano, S. M., Tramblay, Y., Reig, F., González-Hidalgo, J. C., Beguería, S., Brunetti, M., Kalin, K. C., Patalen, L., Kržič, A., Lionello, P., Lima, M. M., Trigo, R. M., El-Kenawy, A. M., Eddenjal, A., Türkes, M., Koutroulis, A., Manara, V., Maugeri, M., Badi, W., … Potopová, V. (2025). High temporal variability not trend dominates Mediterranean precipitation. Nature. https://doi.org/10.1038/s41586-024-08576-6

Voldoire, A., Saint-Martin, D., Sénési, S., Decharme, B., Alias, A., Chevallier, M., Colin, J., Guérémy, J. -F., Michou, M., Moine, M. -P., Nabat, P., Roehrig, R., Salas Y Mélia, D., Séférian, R., Valcke, S., Beau, I., Belamari, S., Berthet, S., Cassou, C., … Waldman, R. (2019). Evaluation of CMIP6 DECK Experiments With CNRM-CM6-1. Journal of Advances in Modeling Earth Systems, 11(7), 2177–2213. https://doi.org/10.1029/2019MS001683

Wang, Y., Zhao, T., Hua, L., Guan, X., Xu, C., & Chen, Q. (2023). Influence of anthropogenic and natural forcings on future changes in precipitation projected by the CMIP6–DAMIP models. International Journal of Climatology, 43(8), 3892–3906. https://doi.org/10.1002/joc.8064

Wild, M. (2012). Enlightening Global Dimming and Brightening. Bulletin of the American Meteorological Society, 93(1), 27–37. https://doi.org/10.1175/BAMS-D-11-00074.1

Wilks, D. S. (2006). Statistical methods in the atmospheric sciences (2nd ed). Academic Press.

Wilks, D. S. (2019). Statistical methods in the atmospheric sciences (Fourth edition). Elsevier.

Wu, T., Yu, R., Lu, Y., Jie, W., Fang, Y., Zhang, J., Zhang, L., Xin, X., Li, L., Wang, Z., Liu, Y., Zhang, F., Wu, F., Chu, M., Li, J., Li, W., Zhang, Y., Shi, X., Zhou, W., … Hu, A. (2021). BCC-CSM2-HR: A high-resolution version of the Beijing

https://doi.org/10.5194/egusphere-2026-2830
Preprint. Discussion started: 11 June 2026
© Author(s) 2026. CC BY 4.0 License.

Climate Center Climate System Model. Geoscientific Model Development, 14(5), 2977–3006. https://doi.org/10.5194/gmd-14-2977-2021

Xoplaki, E., González-Rouco, J. F., Luterbacher, J., & Wanner, H. (2004). Wet season Mediterranean precipitation variability: Influence of large-scale dynamics and trends. Climate Dynamics, 23(1), 63–78. https://doi.org/10.1007/s00382-004-0422-0

Yukimoto, S., Kawai, H., Koshiro, T., Oshima, N., Yoshida, K., Urakawa, S., Tsujino, H., Deushi, M., Tanaka, T., Hosaka, M., Yabu, S., Yoshimura, H., Shindo, E., Mizuta, R., Obata, A., Adachi, Y., & Ishii, M. (2019). The Meteorological Research Institute Earth System Model Version 2.0, MRI-ESM2.0: Description and Basic Evaluation of the Physical Component. Journal of the Meteorological Society of Japan. Ser. II, 97(5), 931–965. https://doi.org/10.2151/jmsj.2019-051

Ziehn, T., Chamberlain, M. A., Law, R. M., Lenton, A., Bodman, R. W., Dix, M., Stevens, L., Wang, Y.-P., & Srbinovsky, J. (2020). The Australian Earth System Model: ACCESS-ESM1.5. Journal of Southern Hemisphere Earth Systems Science, 70(1), 193–214. https://doi.org/10.1071/ES19035